

Brightness perception, illusory contours, and corticogeniculate feedback

ALAN GOVE,¹ STEPHEN GROSSBERG,² AND ENNIO MINGOLLA²

¹MIT Lincoln Laboratory, 244 Wood Street, Lexington

²Department of Cognitive and Neural Systems and Center for Adaptive Systems, Boston University, Boston

(RECEIVED November 30, 1994; ACCEPTED April 4, 1995)

Abstract

A neural network model is developed to explain how visual thalamocortical interactions give rise to boundary percepts such as illusory contours and surface percepts such as filled-in brightnesses. Top-down feedback interactions are needed in addition to bottom-up feed-forward interactions to simulate these data. One feedback loop is modeled between lateral geniculate nucleus (LGN) and cortical area V1, and another within cortical areas V1 and V2. The first feedback loop realizes a matching process which enhances LGN cell activities that are consistent with those of active cortical cells, and suppresses LGN activities that are not. This corticogeniculate feedback, being endstopped and oriented, also enhances LGN ON cell activations at the ends of thin dark lines, thereby leading to enhanced cortical brightness percepts when the lines group into closed illusory contours. The second feedback loop generates boundary representations, including illusory contours, that coherently bind distributed cortical features together. Brightness percepts form within the surface representations through a diffusive filling-in process that is contained by resistive gating signals from the boundary representations. The model is used to simulate illusory contours and surface brightnesses induced by Ehrenstein disks, Kanizsa squares, Glass patterns, and café wall patterns in single contrast, reverse contrast, and mixed contrast configurations. These examples illustrate how boundary and surface mechanisms can generate percepts that are highly context-sensitive, including how illusory contours can be amodally recognized without being seen, how model simple cells in V1 respond preferentially to luminance discontinuities using inputs from both LGN ON and OFF cells, how model bipole cells in V2 with two colinear receptive fields can help to complete curved illusory contours, how short-range simple cell groupings and long-range bipole cell groupings can sometimes generate different outcomes, and how model double-opponent, filling-in and boundary segmentation mechanisms in V4 interact to generate surface brightness percepts in which filling-in of enhanced brightness and darkness can occur before the net brightness distribution is computed by double-opponent interactions.

Keywords: Brightness, Illusory contours, Lateral geniculate nucleus, Visual cortex, Neural networks, Adaptive resonance theory

Introduction

This article describes a previously unsuspected linkage between the mechanisms of binocular vision, illusory contour formation, and brightness perception that was first reported in Gove et al. (1994). The binocular vision mechanisms include corticogeniculate feedback pathways, one of whose functional roles is hypothesized to be the selection of monocular LGN cells whose activation is consistent with that of cortical cells that are activated during binocular and monocular viewing (Grossberg, 1976, 1980; Murphy & Sillito, 1987; Singer, 1979). We propose that this feedback from cortical area V1 to the LGN has testable effects on the brightness percepts that are generated along

with certain illusory contours. A neural model of these LGN-V1 interactions is developed and used, as part of a larger theory, to simulate the illusory brightening and darkening effects that are generated along with illusory contours in response to Ehrenstein, Kanizsa, Glass, and café wall input patterns. In some of these patterns (the single contrast patterns), all of the inducing image elements have the same sign with respect to the image background. In other patterns (the mixed contrast and reverse contrast patterns), some inducing elements have opposite contrasts with respect to the background. Correlated changes in brightness and contour percepts in response to both types of patterns are simulated using the model.

We have selected this particular set of data for analysis because it presents conceptual challenges to all models of visual perception. For example, how are curved, even circular, illusory contours generated from just a few image contrasts, none of which is colinear with the contour (Fig. 1A)? How are illusory

Reprint requests to: Stephen Grossberg, Department of Cognitive and Neural Systems and Center for Adaptive Systems, 111 Cummington Street, Boston, MA 02115, USA.

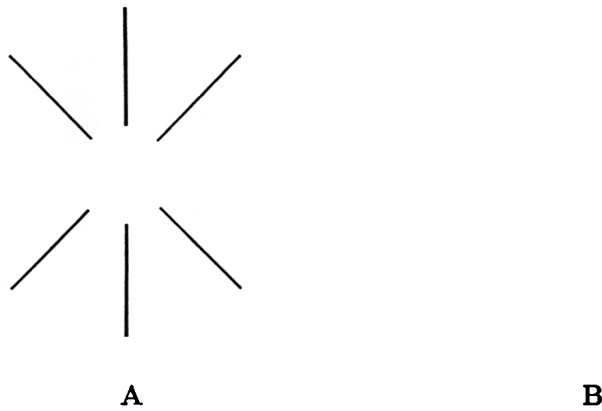


Fig. 1. (A) Ehrenstein illusion: The circular illusory contour encloses a disk of enhanced brightness. The different brightnesses inside and outside the circle render the disk visible. (B) A vertical illusory contour is readily recognized even though it is not "seen" in the sense of separating two regions of different brightness and color.

contours recognized even if they do not separate an image into two regions of visibly different brightness or color (Fig. 1B)? How do illusory contours *sometimes* separate an image with constant background luminance into two regions of different brightness or color (Fig. 1A)? How is the relative brightnesses of the two regions determined? All of these questions illustrate more general issues concerning how the visual system generates boundary and surface representations, of which illusory contours and brightness percepts provide particularly compelling examples. For a review of the functional significance of illusory contours and brightness percepts in the broader scheme of visual boundary and surface representation, see Grossberg (1994) and Grossberg et al. (1989).

The perception of "brightness buttons" at line ends

The interior of the Ehrenstein disk that is surrounded by the illusory contour in Fig. 1A is brighter than its exterior. This apparently simple percept has attracted a great deal of attention from vision scientists because one could imagine many reasons why no brightness difference or the reverse brightness difference might have been seen instead (Leshner, in press). Kennedy (1979) has attempted to explain this percept by positing that "brightness buttons" occur at the ends of dark (low luminance) lines. Other authors have used terms such as "dissimilation" or "line end contrast" to describe this perceptual phenomena, which has long been thought to be distinct from classical "area" contrast, whereby the luminance that engenders perceptual contrast in a target region completely encloses its area (Frisby & Clatworthy, 1975; Day & Jory, 1978; Halpern, 1981). The textbook mechanism for explaining brightness (area) contrast has, in turn, for decades been an appeal to the on-center, off-surround receptive fields of early visual processing.

An analysis of how such cells respond to dark lines shows, however, that they cannot, by themselves, explain brightness buttons. More generally, neither on-center off-surround cells (called ON cells below) nor off-center on-surround cells (called OFF cells below) can explain this phenomenon. We interpret this to mean that the ON and OFF cells that occur in the LGN (Schiller, 1992), and that are the source of cortical brightness percepts (De Yoe & van Essen, 1988) cannot, without further processing, explain brightness buttons. Fig. 2 shows that whatever contribution to area contrast is generated at the ends of thin lines by ON or OFF cells must be less in magnitude than that generated along their sides. As explained below, this should

make the Ehrenstein disk appear darker, rather than brighter, than its surround.

To see why this is so, assume as in Fig. 2B that the thin line is black (low luminance) and surrounded by a white (high luminance) background. Since OFF cells respond best to low lumi-

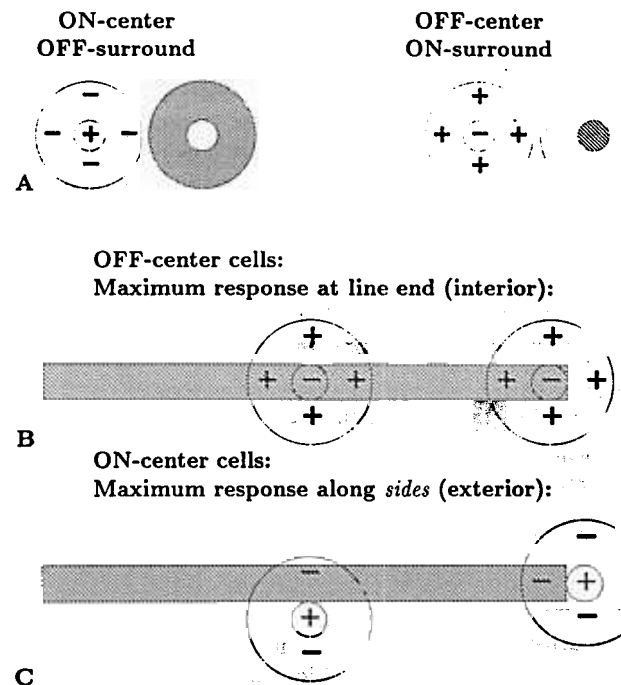


Fig. 2. Retinal center-surround cells and their optimal stimuli (A). The ON cell, on the left, responds best to a high luminance disk surrounded by a low luminance annulus. The OFF cell, on the right, responds best to a low luminance disk surrounded by a high luminance annulus (B). OFF cells respond to the inside of a black line. The OFF cell centered at the line end responds more strongly than the OFF cell centered in the middle, because the surround region of the former cell is closer to optimal. In (C) ON cells respond to the white background just outside the black line. The amount of overlap of each ON cell's surround with the black line affects the strength of the cell's response. As seen in the ON cell's optimal stimulus (C), the more of the surround that is stimulated by a black region, the better the ON cell will respond. Thus, an ON cell centered just outside the side of the line will respond better than a cell centered just outside the end of the line.

nance in their receptive-field center and high luminance in their surround, OFF cells whose centers lie inside the line will be activated. Furthermore, OFF cells near the line end (but still inside the line) will be more strongly activated than OFF cells in the middle of the line, because the line end is more like a black disk surrounded by a white background than the line middle is (Fig. 2B). That is, an OFF cell whose center lies in the line end receives less inhibition from its surround than does a cell centered in the middle of the line, because a larger area of the former cell's surround lies in the white background.

A similar analysis can be applied to the ON cells. An ON cell is excited by high luminance in the center of its receptive field and low luminance in its surround. The ON cells that are active, then, are those centered outside the bar. An ON cell whose center is just outside the side of the line will respond more strongly than an ON cell centered just outside the end of the line (Fig. 2C).

Given that LGN ON and OFF cells, by themselves, cannot explain brightness buttons, it still remains to explain how a brighter Ehrenstein disk could be generated were brightness buttons to obtain. Clues were provided by Kennedy (1979), who analyzed a number of illusory contour stimuli. He argued that the effect of brightness buttons could often go unnoticed for isolated line segments, but could somehow be pooled and amplified in perceptual salience when several brightness buttons occurred in proximity or within a figurally complete region (see Fig. 3). Grossberg and Mingolla (1985a) presented an analysis and interpretation of Kennedy's remarks through their development of a neural model of visual boundary and surface representation. In their model, the crucial mechanistic support for perceptually noticeable brightness buttons is a boundary segmentation that separates the region containing the buttons from other regions of a scene. Such a boundary segmentation may be generated by image edges, textures, or shading, and may give rise to illusory contours. Boundary segmentation within the model is accomplished by the filtering, competitive, and cooperative interactions of a grouping network called the Boundary Contour System, or BCS.

The boundaries within the BCS do not carry a perceptually visible signal. As explained in greater detail below, BCS outputs are rendered insensitive to contrast polarity by pooling boundary signals that are sensitive to opposite contrast polarities. Visible brightness and color percepts are assumed to emerge

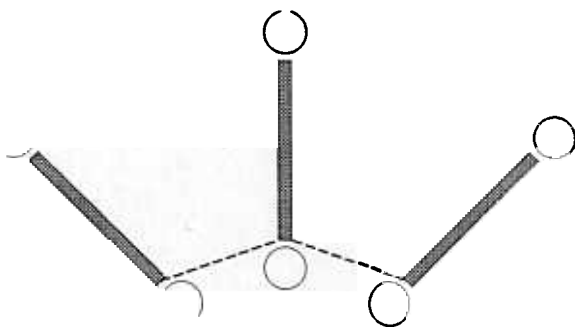


Fig. 3. Brightness buttons lie outside thin lines. When the induced boundary contour (denoted by the dashed line) lies on one side of the buttons, their perceptual effect is enhanced. If the induced boundary instead divided the brightness buttons, they would have less of a perceptual effect.

in a surface representation system that is called the Feature Contour System, or FCS. Output signals from the BCS form compartments within the FCS, within which LGN inputs to the FCS initiate a diffusive filling-in process that generates a surface representation, including a percept of brightness. In the complete binocular BCS/FCS model (Grossberg, 1994), this surface representation emerges only after several stages of BCS and FCS interaction occur. The model simulated herein has been simplified to focus upon the targeted data base.

The full BCS models aspects of the interblob cortical processing stream from area V1 to V4, and the FCS models the blob processing stream (see Grossberg, 1994, for a review). Many brightness data have been simulated within this modeling framework (Andreou & Boahen, 1991; Arrington, 1994; Cohen & Grossberg, 1984; Grossberg & Todorović, 1988; Pessoa et al., 1994). Lacking in these accounts, however, was a mechanism for generating the distribution of brightness inputs that could underlie the perceptual phenomena associated with brightness buttons. In particular, previous versions of the BCS/FCS model incorrectly predicted that the Ehrenstein disk should look darker than its surround. Given that so many brightness data had been correctly predicted by the model, including data collected after its publication (Arrington, 1994; Paradiso & Nakayama, 1991; Watanabe & Sato, 1989; Watanabe & Takeichi, 1990), the question arose of how the model's description was incomplete or incorrect. Such an account is developed in the present work, which shows how the addition of the corticogeniculate feedback loop helps to explain brightness buttons without disturbing the model's previous explanations of other brightness phenomena.

The gist of the present model can be summarized as follows. Brightness buttons are by definition an effect of an *oriented* structure (such as a line, or more generally a corner or sharp bend in a contour) on perceived featural quality (brightness). Within the prior versions of the BCS and FCS model equations, the computations of the FCS were unoriented, in the sense that they were mediated either by cells with circularly symmetric kernels governing their processing of inputs from a prior stage, or by an isotropic diffusion. How then could the effects of *oriented* filtering be used to modulate the inputs to the FCS that produce brightness buttons? Indeed, oriented filtering alone could not suffice. Interactions must exist among the oriented filters to determine the location of the ends of the lines, at which the brightness buttons occur. A natural candidate for the latter interactions is the endstopping process that converts cortical complex cells into endstopped complex, or hypercomplex, cells (Hubel & Wiesel, 1977). Where should the results of this endstopped processing have their effect on inputs to the FCS?

Having come this far, it is plausible to propose that the cortex influences LGN cells *via* top-down feedback, which it is well known to do (Guillery, 1967). It is not plausible, however, that this massive feedback pathway exists just to make Ehrenstein disks appear bright. Grossberg (1976, 1980) suggested that corticogeniculate feedback exists for a potentially important functional reason; namely, to enhance the activity of LGN cells that support the activity of presently active cortical cells, and to suppress the activity of LGN cells that do not. In addition, bottom-up retinal input, by itself, was hypothesized to supraliminally activate LGN cells, but top-down corticogeniculate feedback, by itself, was not.

These rules realize a type of matching that has been proposed in Adaptive Resonance Theory, or ART; see Carpenter and Grossberg (1991, 1993) for reviews. In this theory, matched

bottom-up and top-down thalamocortical signal exchanges coherently bind and synchronize the activities of cells whose features code the same object part or other unitized event. Once coherence or resonance is achieved, learning of new tuning curves or associations is triggered. The reciprocal matching interactions between LGN and cortex were thereby proposed to control and stabilize adaptive synaptic changes in response to the flood of visual experience. As noted below, Sillito et al. (1994) have reported neurophysiological LGN data that are consistent with these model predictions. The following sections describe how this feedback pathway can also subserve the formation of brightness buttons, as an epiphenomenon of its posited primary functional role. Said another way, this analysis predicts that a weakening of top-down feedback could generate dark Ehrenstein disks while removing oriented influences on LGN cells and destabilizing the adaptive tuning of binocular cortical cells, assuming that the rest of the cortex is still functional.

Brightness button signals can, in fact, be generated in two ways that are consistent with reported physiology: (1) Excitatory feedback from cortical endstopped cells can enhance LGN cell activity near line ends. (2) Net inhibitory feedback from long-field cells, modulated by LGN interneurons, can suppress activity in LGN cells coding the sides of lines, making brightness contrast at line ends relatively stronger. A combination of the two mechanisms would have the same properties. Data available at present favor the first hypothesis, and that is the one investigated in the present work.

Model LGN circuit

The model LGN ON and OFF cells receive input from retinal ON and OFF cells. (See Schiller, 1992, for a review.) Because these ON and OFF cells have antagonistic surrounds and obey shunting, or membrane, equations (see the Appendix), they help to discount the illuminant, normalize image activities, and extract ratio contrasts from an image (Grossberg, 1983). These image preprocessing properties are needed to simulate even the most basic brightness percepts (Grossberg & Todorović, 1988). As a result of these mechanisms, ON and OFF cells process line ends in the manner summarized in Fig. 2. Other properties of the LGN, such as the existence of M and P channels and of lagged cells, are not needed to explain the targeted data, and so are omitted for simplicity.

The LGN model also receives feedback from model cortical cells, and this feedback can cause the resultant LGN activity to differ under certain circumstances from that caused solely by its retinal input. For instance, the feedback signals increase both ON and OFF activity near line ends and other areas of sharp boundary discontinuity (Fig. 4). This increase in activity of ON and OFF relay cells is effectively an increase in ON-OFF contrast, which is manifested after filling-in within the FCS as an increase in brightness contrast. This is the model analog of "brightness buttons" (Kennedy, 1979) and of "line end contrast" (Day & Jory, 1978). The increased LGN activity at the line end can also better activate cortical simple cells located at the line end, resulting in stronger boundary formation perpendicular to the line end, as in the circular illusory contour of Fig. 1A, than would otherwise be the case.

In the model, cortical feedback to LGN cells derives from a population of endstopped cells; namely, from the outputs of the first hypercomplex (endstopped) cell stage of the BCS (Fig. 5A). These cells excite relay cells in the LGN whose receptive-field

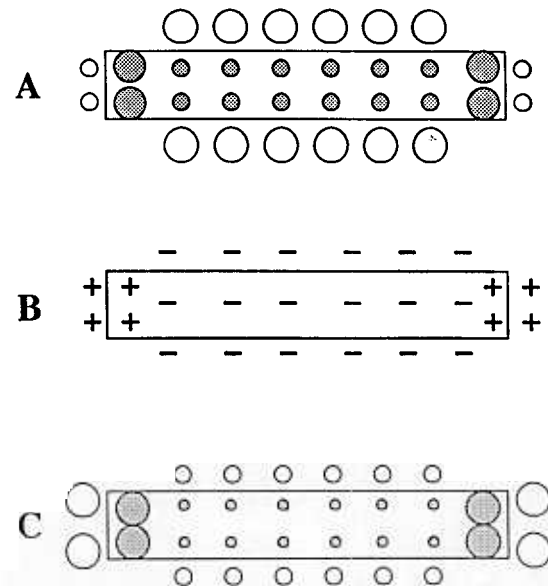


Fig. 4. Schematic diagram of brightness button formation in the model. In (A) the distribution of model LGN cell activities prior to receiving any feedback, in response to a black bar, is illustrated. Open circles code ON cell activity; filled circles code OFF cell activity. (B) shows the effect of feedback on bottom-up LGN activations. (C) shows the LGN activity distribution after feedback. A brightness button is formed outside both ends of the line. Also note that a vertically oriented simple cell receiving input from the line end will be more strongly activated after this transformation, which can help produce stronger endcuts.

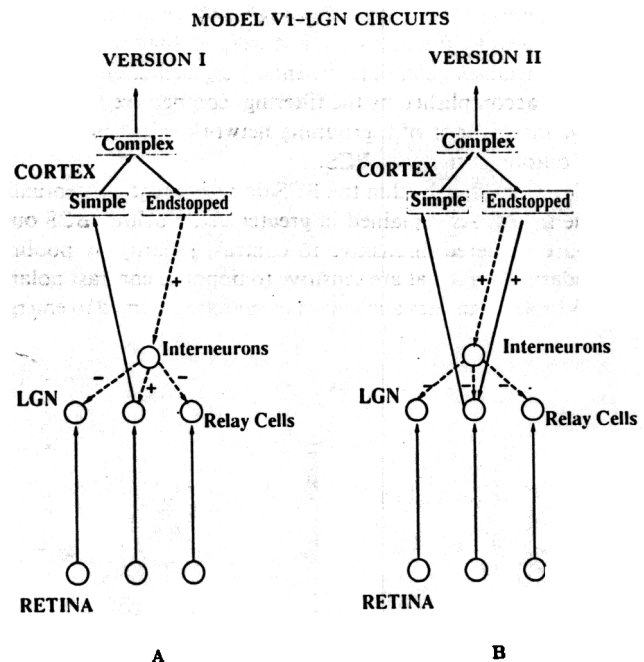


Fig. 5. LGN model diagram. (A) In Version I, feedback signals originate in cortical endstopped cells and enter a center-surround competition within the LGN. (B) In Version II, the feedback from cortical endstopped cells directly excites LGN relay cells (solid line), and also activates LGN interneurons, which inhibit nearby relay cells (dashed lines). Versions I and II are functionally equivalent. Version II was used for simulations.

centers are topographically aligned with their corresponding cortical cells. Nearby relay cells are inhibited by the activity of LGN interneurons. An alternative model implementation is slightly more complicated and reflects more closely the corticogeniculate feedback seen in the cat (Fig. 6). Here, model feedback is sent to both relay cells and LGN interneurons (Dubin & Cleland, 1977; Weber et al., 1989). Both feedback streams are excitatory; however, the interneurons, which become more active due to the feedback, inhibit nearby relay cells (Fig. 5B). The circuit in Fig. 5B achieves the same functional result as that in Fig. 5A, but also obeys Dale's principle that all synaptic targets of a given cell be either excitatory or inhibitory, but not both.

Since endstopped cells respond best to line ends and short line segments, the activity of LGN relay cells near line ends is increased by feedback to these areas. The feedback also activates topographically corresponding interneurons in the LGN, which inhibit relay cells in a local neighborhood. In all, the feedback instantiates a center-surround competition. The inhibitory surround can depress LGN signals in areas away from the line ends, such as along the line sides (Fig. 4B). Since ON and OFF channels are segregated in the LGN (Schiller, 1992), the feedback is applied to the ON and OFF layers separately.

Neurophysiological LGN data

The LGN model is supported by a variety of anatomical and physiological data from studies of the cat and monkey. The LGN is often thought of as a visual relay station between the

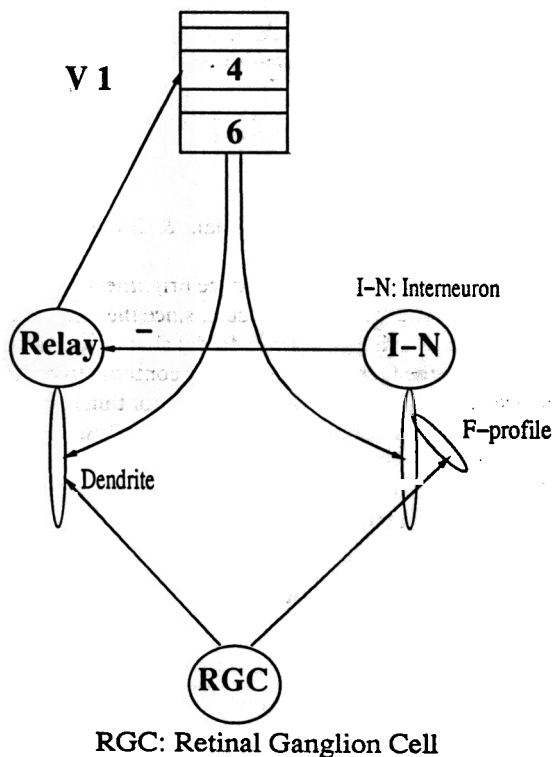


Fig. 6. Schematic diagram of the V1-LGN local circuit. All V1-LGN pathways are excitatory, but some synapse directly on dendrites of relay cells, while others synapse on inhibitory interneurons, at a site distinct from the "F-profile," which receives input from retinal ganglion cells. Adapted with permission from Weber et al. (1989).

retina and visual cortex. However, the LGN also has an intricate local circuitry that is much more complex than a mere relay station would require. There are two basic cell types in the LGN: relay cells and interneurons. For present purposes, extrinsic interneurons located in the perigeniculate nucleus can also be considered LGN interneurons. Retinal ganglion cells project directly to both types of cells (Dubin & Cleland, 1977). While relay cells in turn project to visual cortex, the axons of interneurons remain in the LGN. Unlike relay cells, interneurons stain positively for GABA (Montero & Zempel, 1985) and are therefore believed to have an inhibitory effect on the relay cells they contact (Sillito & Kemp, 1983).

Both LGN cell types receive feedback from layer 6 pyramidal cells in striate cortex (Guillery, 1967). This corticogeniculate feedback is massive, with more fibers going from cortex to LGN than *vice versa*. Of all of the synapses in the LGN, about 50% originate in cortex, compared to only 20% that originate in the retina (Robson, 1983). The feedback, which comes from cells that are binocular and orientation selective (Gilbert & Kelly, 1975), is also topographic, with a strict correspondence between the locations of the visual fields of the bottom-up and top-down signals converging on a LGN cell (Updyke, 1975). If the LGN were just a relay station, there would be no need for the precision or amount of feedback that is seen.

From neurochemical evidence the feedback is believed to be excitatory (Montero, 1990), but since it directly activates both relay cells (Dubin & Cleland, 1977) and interneurons (Weber et al., 1989), the overall effect of feedback on the LGN is hard to predict from the known anatomy (see Fig. 6). Neurophysiologists have also had difficulty in assessing the function of the corticogeniculate feedback. Researchers trying to measure the effect of feedback on LGN transmission of retinal signals have met with inconsistent results. Some studies have found excitatory effects (e.g. Kalil & Chase, 1970), while others have found inhibitory effects (e.g. Hull, 1968), and still others found mixed excitatory and inhibitory effects (Marrocco & McClurkin, 1985).

The modulation of cat LGN by cortical feedback changes with arousal level and brain-stem activity (Funke & Eysel, 1992). The feedback can serve as a gain control mechanism for the entire thalamus, boosting the gain of signals from one modality while suppressing signals from other modalities. This cannot be the only purpose, however, as it would not justify such a large and complex feedback system; a global arousal signal would suffice.

Corticogeniculate feedback is also involved in cortical binocular processing (Grossberg, 1976, 1980; Singer, 1977; Varela & Singer, 1987). As noted above, Grossberg (1976, 1980) suggested that the feedback pathway realizes a top-down pattern matching process that helps to selectively amplify activities of monocular LGN cells that support the activities of binocular cortical cells, and to suppress the activities of LGN cells that do not, *via* positive corticogeniculate feedback linked to internal LGN opponent processes. Topographic correspondence is necessary to carry out such a matching process. A similar modulatory role for top-down feedback is assumed to be active during monocular viewing.

This role for corticogeniculate feedback was hypothesized to be part of a more general and ubiquitous model of top-down feedback in stabilizing adaptive synapses in thalamocortical and corticocortical circuits, while also regulating the gain of these circuits. In this more general Adaptive Resonance Theory, or ART, modeling framework, bottom-up processing in the ab-

sence of top-down processing can activate its target circuits, top-down processing represents a form of hypothesis testing that can subliminally prime these circuits, and a combination of bottom-up and top-down processing can select those bottom-up activations that are consistent with top-down feedback and suppress those that are not. This more general role for top-down processing is consistent with the fact that corticogeniculate feedback is present in all parts of the visual field, not just the portion with binocular overlap, and the feedback is also present in species with little or no binocular overlap (Koch, 1987).

In striking support of this ART prediction, Sillito et al. (1994) reported that "cortically induced correlation of relay cell activity produces coherent firing in those groups of relay cells with receptive-field alignments appropriate to signal the particular orientation of the moving contour to the cortex . . . this increases the gain of the input for feature-linked events detected by the cortex . . . the cortico-thalamic input is only strong enough to exert an effect on those dLGN cells that are additionally polarized by their retinal input . . . the feedback circuit searches for correlations that support the 'hypothesis' represented by a particular pattern of cortical activity" (pp. 479–482).

Because corticogeniculate feedback has both excitatory and inhibitory (*via* interneurons) components, the cortex can selectively suppress or enhance particular features of an image. One feature known to be affected is stimulus length. Murphy and Sillito (1987) showed that cortical feedback causes significant length-tuning in cat LGN cells. As in cortical endstopping, the response to a line grows rapidly as a function of line length and then abruptly declines for longer lines. The response to long lines is hereby depressed. Redies et al. (1986) found that cat dorsal LGN cells and strongly endstopped cortical complex cells responded best at line ends, both for single lines and for a set of parallel lines shifted to form a perpendicular illusory contour, as in Fig. 7A. In other words, the response of the LGN cells to line ends was enhanced relative to the response to line sides. Computer simulations described below show that the model corticogeniculate feedback is also length-tuned and enhances line ends, as seen in the data of Redies et al. (1986) and Murphy and Sillito (1987).

LGN stage predictions

By enhancing LGN responses at line ends, model corticogeniculate feedback also increases the input to model cortical simple cells whose preferred orientations are perpendicular to the line end. These perpendicular activations, called endcuts, help to initiate the formation of illusory contours in an orientation that is perpendicular to the line ends, as in Fig. 1A. Computer simulations have shown that the width and orientation of the line end are important parameters for determining illusory contour and brightness strength. If a line end is too thin, then enhanced LGN contrast at the line end is not sufficient to activate a cortical simple cell oriented perpendicular to the line, and thus boundaries induced by very thin lines should be weakened, as illustrated in Fig. 7A.

The orientation of a line end need not be perpendicular to the line, and the model predicts that, other things equal, boundary completion should occur preferentially along the contour of the line end, as in Fig. 7B, because that is the orientation of the maximally activated simple cell. The general preference for perpendicular completion is a local effect that may be overridden by global cues for three-dimensional surface formation

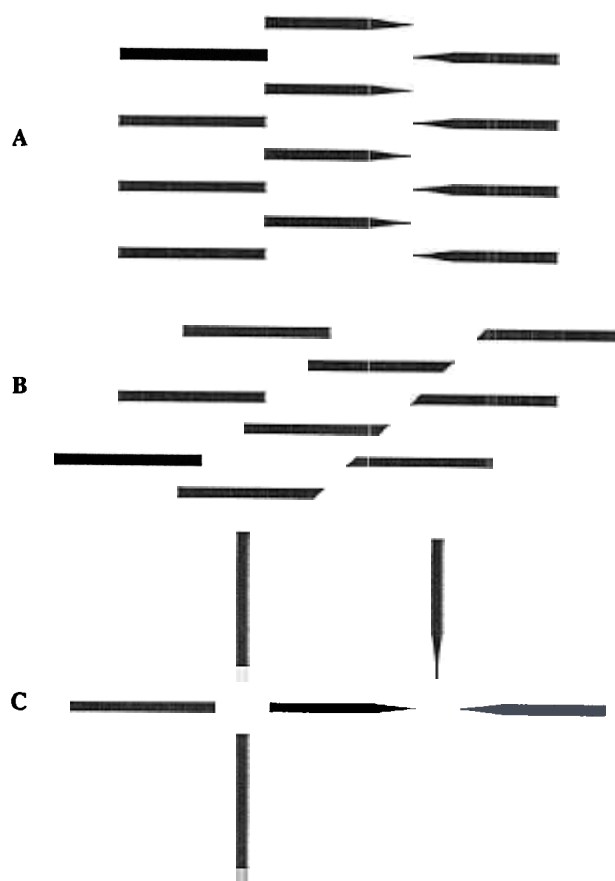


Fig. 7. Some examples of the effects of line end shape on boundary completion strength and brightness. (A) Very thin lines do not induce strong completions. (B) Completions are best when they are aligned with the contour of the line end. (C) Thin line ends can produce a "glow" that is predicted by the LGN model. Patterned after Kennedy (1988).

and figure-ground separation (Gillam & Goodenough, 1994; Grossberg, 1994).

A thin line is predicted to produce brightness buttons, even if it does not produce strong endcuts, since the LGN relay cells near the line end will be excited by feedback, as in Fig. 7C. However, because the formation of illusory contours to contain the enhanced brightness signals is suboptimal for thin line ends, any noticeable brightness difference may be diffuse rather than sharp. Kennedy (1988) has studied these various effects of line ends on illusory contours and brightness, and his results are consistent with the analysis outlined above.

A unified explanation of illusory contour and brightness properties

Fig. 8 summarizes the macrocircuit of the LGN-cortical model that is simulated herein. The model includes ON and OFF retinal and LGN cells; cortical simple, complex, hypercomplex, higher-order hypercomplex, and bipole cells of the cortical interblob processing stream; and ON and OFF opponent and double-opponent filling-in cells of the cortical blob processing stream. Using this model system, a set of simulations was carried out with a fixed set of parameters to illustrate how the model emulates a wide range of illusory contour and brightness percepts.

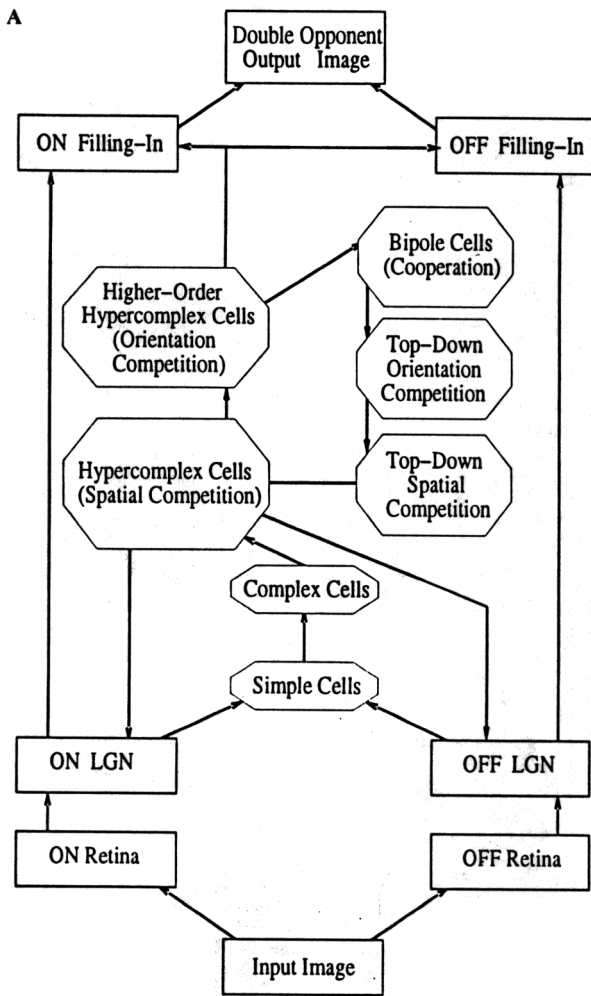
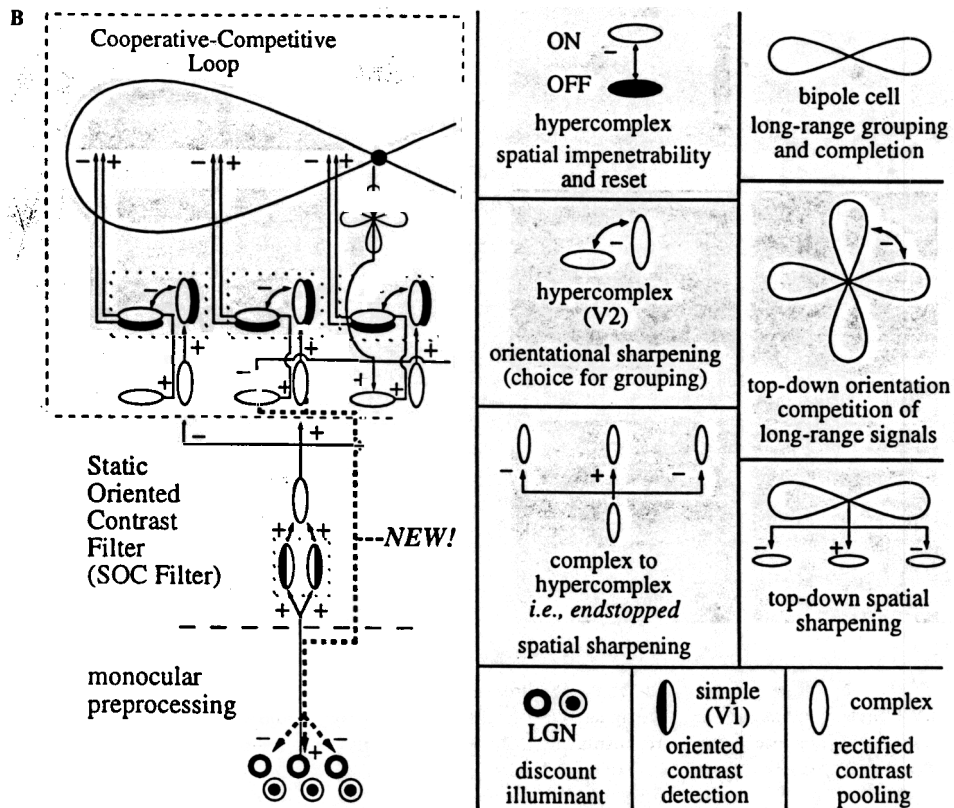


Fig. 8. (A) Model macrocircuit. BCS stages are designated by octagonal boxes, FCS stages by rectangular boxes. (B) Model stages schematized by cell icons and intercellular circuits. While most of the terms used are self-explanatory or explained in the text, “spatial impenetrability” refers to the need to prevent the cooperative bipole cells from forming spurious or inappropriate groupings where local evidence overrules long-range coalignments, and “reset” refers to the temporal aspects of formation, persistence, and dissolution of perceptual segmentations. Note that the “four leaf clover” icon in the diagram is not drawn to scale, but represents competition among long-range bipoles, such as the one partially depicted at the top of the CC Loop. See text for details.



Figs. 9–15 summarize simulations of the Ehrenstein disk, the reverse-contrast Ehrenstein disk, the Kanizsa square, the mixed-contrast Kanizsa square, the Glass pattern, the mixed-contrast Glass pattern, and the café wall illusion, respectively. In each figure, panel (A) represents the input image, panel (B) the LGN activation pattern, panel (C) the boundary segmentation, and panel (D) the filled-in surface representation. To comment further about the simulations, the model stages depicted in Fig. 8 and their functional role will be described qualitatively, including a description of how the present version of the model refines previous versions. Then some key properties of the simulated percepts will be further discussed. The model is described mathematically in the Appendix, along with details of how the computer simulations were carried out.

Model overview

We illustrate model dynamics by tracing how different modeling stages respond to two black horizontal bars on a light background delivered to the model retina. In Fig. 16, the small circles represent small luminances, the large circles large luminances, at the corresponding image pixels. This image is transformed

by the model retinal and LGN ON and OFF cells as shown in Fig. 17. Note that the representations of LGN activity in panel (B) of Figs. 9–15 indicate both ON and OFF activity, as in Fig. 17, but with a middle gray placed in locations having no circle in Fig. 17.

The LGN cell outputs activate the first stage of cortical BCS processing, the simple cells (see Fig. 8) whose oriented receptive fields respond to a prescribed contrast polarity, or direction-of-contrast. The model LGN cells input to pairs of like-oriented simple cells that are sensitive to opposite directions-of-contrast. The simple cell pairs, in turn, send their rectified output signals to like-oriented complex cells. By pooling outputs from oppositely polarized simple cells, complex cells are rendered insensitive to direction-of-contrast, as are all subsequent BCS cell types in the model.

Complex cells activate hypercomplex cells through an on-center off-surround network, or spatial competition, whose off-surround carries out an endstopping operation (see Fig. 18B). In this way, complex cells excite hypercomplex cells of the same orientation and position, while inhibiting hypercomplex cells of the same orientation at nearby positions. One role of this spatial competition is to spatially sharpen the neural responses

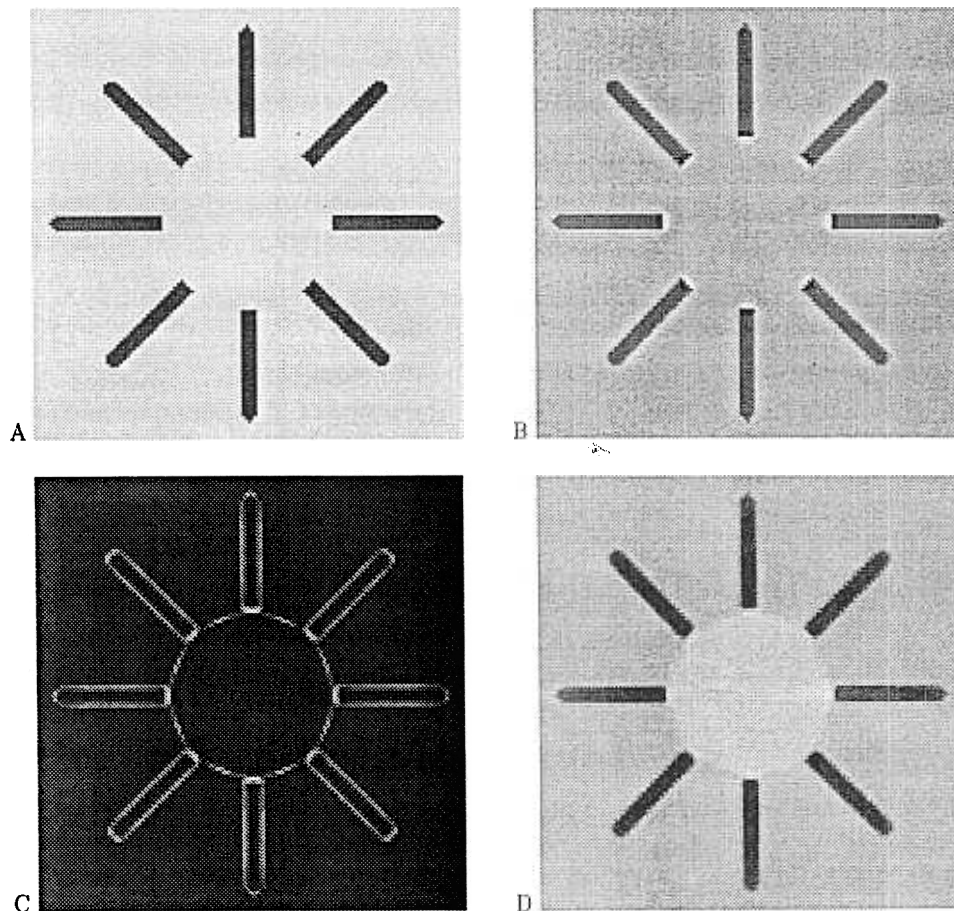


Fig. 9. (A) The Ehrenstein figure. (B) The LGN stage response. Both ON and OFF activities are coded as rectified deflections from a neutral gray. Note the brightness buttons at the line ends. (C) The equilibrium BCS boundaries. (D) In the filled-in result, the central circle contains stronger FCS signals than the background, corresponding to the perception of increased brightness. Note that in this and subsequent figures displaying BCS output (including Figs. 9–14), the representation of boundaries at multiple orientations are superimposed. Photographic reduction prohibits inspection of responses of individual orientations, as is apparent in Fig. 18.

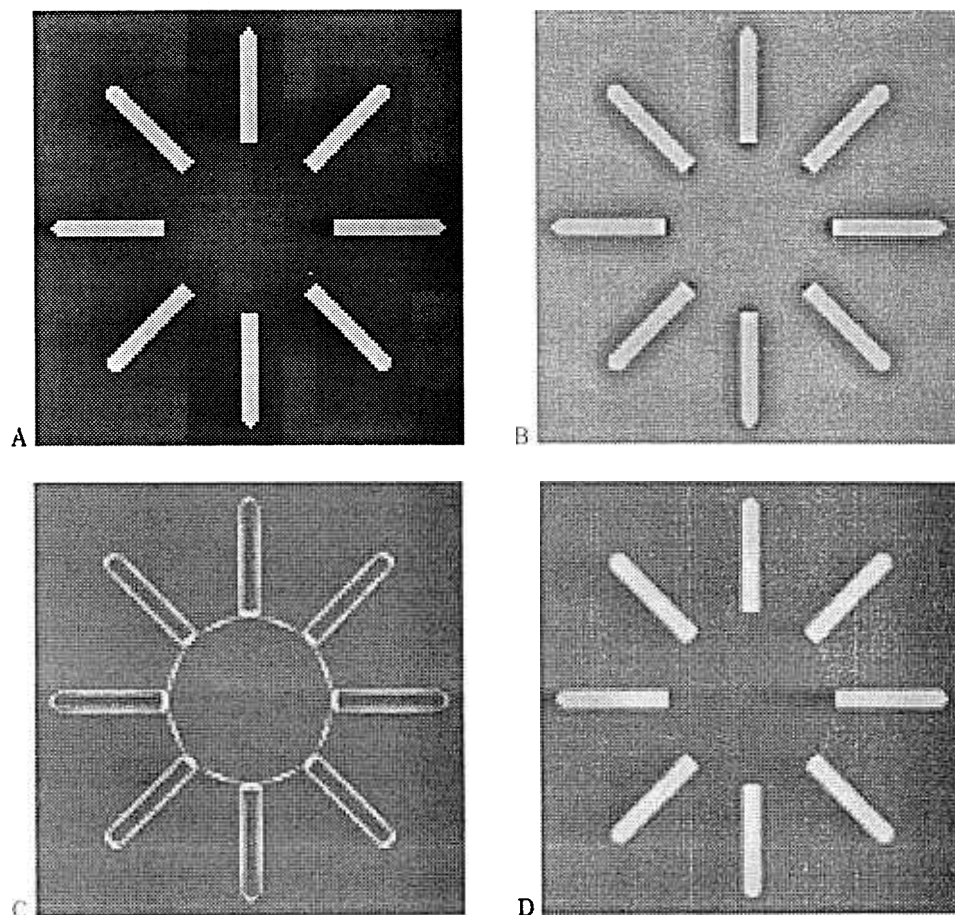


Fig. 10. Inverse Ehrenstein figure. (A) The input image has the luminance values of the original Ehrenstein figure reversed. (B) The LGN stage response. Note that the "brightness" buttons at the line ends are darker than the background; they are "darkness buttons." (C) The equilibrium BCS boundaries are the same as for the standard Ehrenstein figure. (D) In the filled-in result the central circle contains weaker FCS signals than the background. Thus the model correctly predicts that the circle will appear darker than the background.

to oriented luminance edges. Another role is to initiate the process, called *end cutting*, whereby boundaries are formed that abut a line end at orientation perpendicular or oblique to the orientation of the line itself, as in Fig. 9C.

The hypercomplex cells input to a competition across orientations at each position among hypercomplex cells (see Fig. 18C). This competition acts to sharpen up orientational responses at each position. Output from the higher-order hypercomplex cells feed into bipole cells that initiate long-range boundary grouping and completion (see Fig. 18D). Bipole cells have two oriented receptive fields. Their cell bodies fire only if both of their receptive fields are sufficiently activated by appropriately oriented hypercomplex cell inputs. Bipole cells act like a type of statistical and-gate that controls long-range cooperation among the outputs of active higher-order hypercomplex cells. For example, a horizontal bipole cell is excited by activation of horizontal hypercomplex cells that input to its horizontally oriented receptive fields. A horizontal bipole cell is also inhibited by activation of vertical hypercomplex cells.

Output signals from bipole cells feed back to the hypercomplex cells after undergoing two stages of competitive processing. First, bipole cell outputs compete across orientation to

determine which orientation is receiving the largest amount of cooperative support (see Figs. 8 and 18E). The next stage of competition takes place across nearby locations to select the best spatial location of the emerging boundary (see Fig. 18F). These competitive interactions are needed to select and sharpen the best boundary grouping because the bipole cell receptive fields are themselves rather broad. Broad bipole receptive fields are needed because, in many situations, neither the image contrasts to be grouped nor the cortical cells that group them are precisely aligned across space. Broad receptive fields allow the grouping to get started and the competitive interactions sharpen and deform it. Hypercomplex cells that receive the most cooperative support from bipole grouping after cooperative-competitive feedback acts further to excite the corresponding bipole cells.

This cycle of bottom-up and top-down interaction between hypercomplex cells and bipole cells rapidly converges to a final boundary segmentation (see Fig. 18G). Feedback among bipole cells and hypercomplex cells hereby drives a resonant cooperative-competitive decision process that completes the statistically most favored boundaries, suppresses less favored boundaries, and coherently binds together appropriate feature combinations

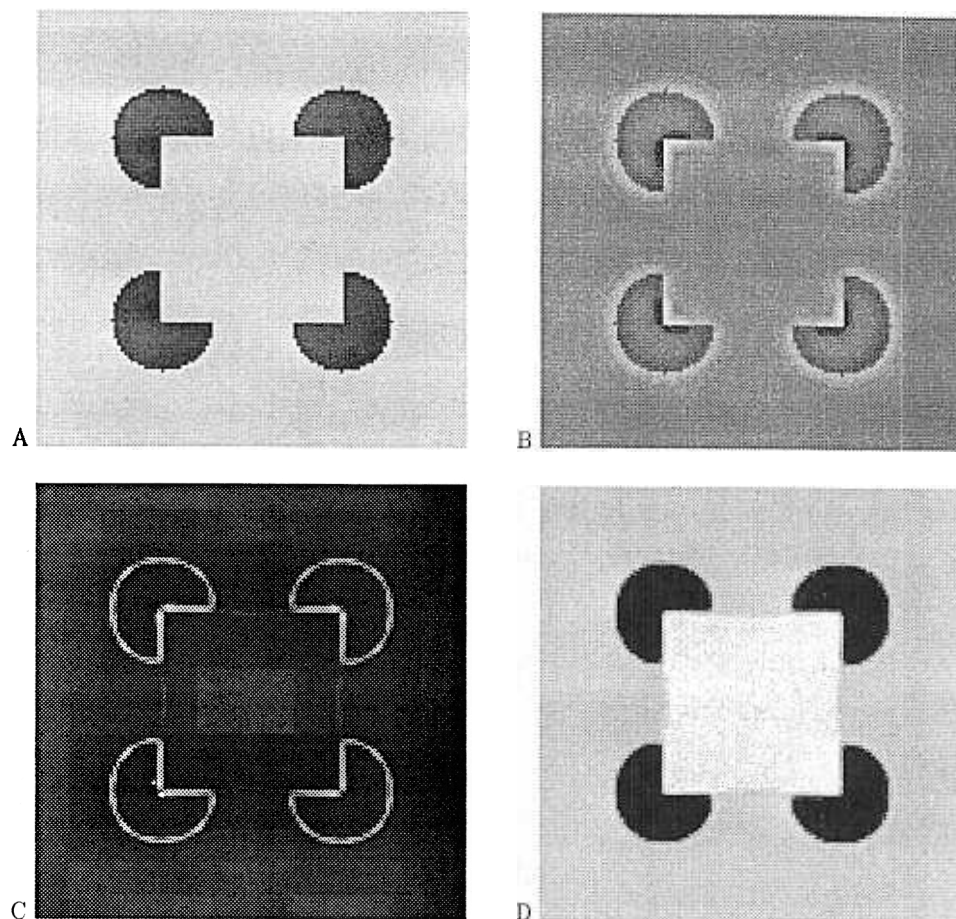


Fig. 11. (A) The Kanizsa square. (B) The LGN stage response. (C) The equilibrium BCS boundaries. (D) In the filled-in result the square contains stronger FCS signals than the background, corresponding to the perception of increased brightness.

in the image. The equilibrium boundary segmentations shown in panel (C) of Figs. 9–15 are all recorded at the higher-order hypercomplex cells.

Each BCS boundary segmentation generates topographic output signals to the ON and OFF Filling-In Domains, or FIDOs (see Fig. 8). These FIDOs also receive inputs from the ON and OFF LGN cells, respectively. The LGN inputs activate their target cells, which allow activation to diffuse rapidly across gap junctions to neighboring FIDO cells. This diffusive filling-in process is restricted to the compartments derived from the BCS boundaries, which create barriers to filling-in by decreasing the permeability of their target gap junctions. The filled-in OFF activities are subtracted from the ON activities at double-opponent cells, whose activities represent the surface brightness of each percept (see Fig. 8). This double-opponent representation is shown in panel (D) of Figs. 9–15 and Fig. 19.

The model in Fig. 8 is simplified relative to known cortical architecture and to known models thereof. It is a single-scale, monocular model. For generalizations to multiple-scale and binocular model interactions, see Grossberg (1994), Grossberg et al. (1994b), and Pessoa et al. (1994). The simulations in Figs. 9–14 are only shown at equilibrium. For simulations of temporal network dynamics, see Arrington (1994), Francis and Grossberg (1994, 1995) and Francis et al. (1994).

Ehrenstein figure simulations

The first simulation (Fig. 9) shows the completions that occur between line segments arranged around a circle in a radial configuration (Ehrenstein, 1941). The input image is shown in Fig. 9A. Fig. 9B shows brightness buttons in the model LGN cell activations. The complex cell responses (see Fig. 8) are strongest at the ends of the line segments, reflecting the effects of the LGN stage. These line end responses are strong enough to induce completions perpendicular to the lines, thereby forming the circular illusory contour (Fig. 9C). Due to the brightness buttons in Fig. 9B, the filled-in surface representation of the central disc in Fig. 9D has stronger activation than the background, which is consistent with the percept generated by this figure in humans (see Fig. 1A).

The results computed by the individual ON and OFF filling-in domains in Fig. 8 are shown in Fig. 20. Some “leakage” across boundaries occurs in the individual ON and OFF filling-in domains, but its effects are effectively cancelled by subtracting the combined output, as shown in Fig. 9D. This combination of ON (on-center off-surround) and OFF (off-center on-surround) cell processing followed by opponent subtraction generates a type of double-opponent receptive field. Grossberg and Wyse (1991) analyzed how double-opponent interactions can cancel leakage

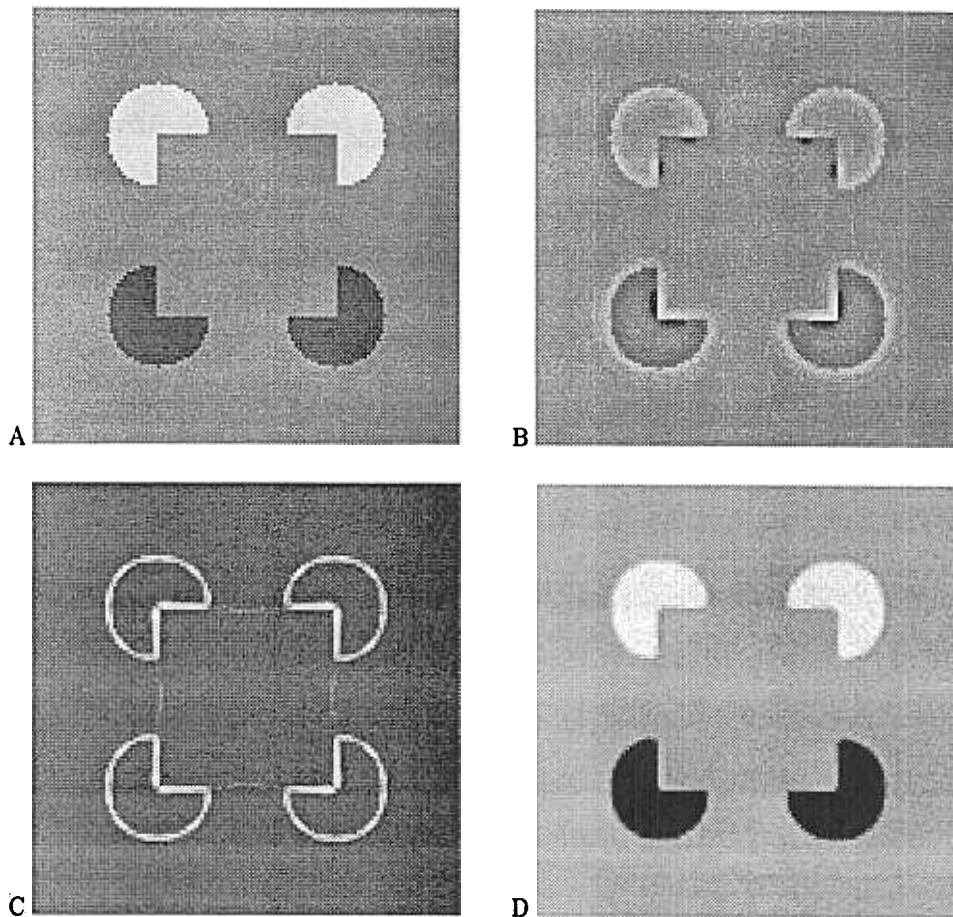


Fig. 12. (A) The mixed contrast Kanizsa square. (B) The LGN stage response. (C) The equilibrium BCS boundaries. (D) The filled-in square contains FCS signals similar to those in the background.

due to filling-in across weak or incomplete boundaries. Some examples of brightness assimilation may be understood as effects of such spreading that, due to figural asymmetries, are *not* cancelled by subsequent ON/OFF interactions.

The Ehrenstein illusion is also simulated with white lines on a dark background. In such a reverse-contrast Ehrenstein figure (Fig. 10A), a circular boundary is generated as in the standard Ehrenstein figure (Fig. 10C), but the interior of the circle appears darker than the background (Fig. 10D). This simulation shows that the mechanisms that generated brightness buttons can also generate “darkness buttons” under appropriate conditions (Fig. 10B). The enhanced darkness spreads in the FCS during filling-in to produce a dark circle.

Kanizsa square simulations

Fig. 11 shows the simulation of a Kanizsa square. The LGN stage generates “brightness corners” at the interior corner of each pac man figure that are enhanced relative to the complex cell output computed in absence of the LGN stage (not shown). The boundaries of the square are completed by cooperative-competitive feedback among the hypercomplex and bipole cells in response to the pac man boundaries (Fig. 11C). The enhanced brightness of the square (Fig. 11D) is caused by filling-in of the brightness corners in Fig. 11B within the square boundary.

In the mixed-contrast Kanizsa square (Fig. 12A), pairs of pac man figures have opposite contrast with respect to the background. Under suitable viewing conditions, most subjects recognize the completed outline of a square in the center of this figure, as in Fig. 12C, although any visible brightness enhancement on one side of the square boundary is greatly reduced, as in Fig. 12D. This illusion is important for at least two reasons. First, it illustrates in a particularly vivid setting that long-range boundary completion (and thus illusory contours) can occur between elements of opposite contrast. Second, the figure produces an illusory contour but not a strong brightness effect. In Fig. 12D, the square is filled-in with approximately the same brightness level as that in the background. Human percepts are consistent with this simulation.

A mixed-contrast Kanizsa square can generate an illusory square that can be *recognized* (Fig. 12C) without necessarily generating a brightness difference within that square that can be *seen* (Fig. 12D). This fact has historically caused a great deal of controversy as the distinction between seeing and thinking, or the related distinction between modal and amodal perception (Coren & Harland, 1993; Epstein, 1993; Gregory, 1993; Kanizsa, 1979; Kellman & Shipley, 1991; Michotte et al., 1964). Within the present theory, this property follows from the fact that boundaries within the BCS carry no perceptual sign — “all boundaries are invisible” — because the outputs of the BCS pool

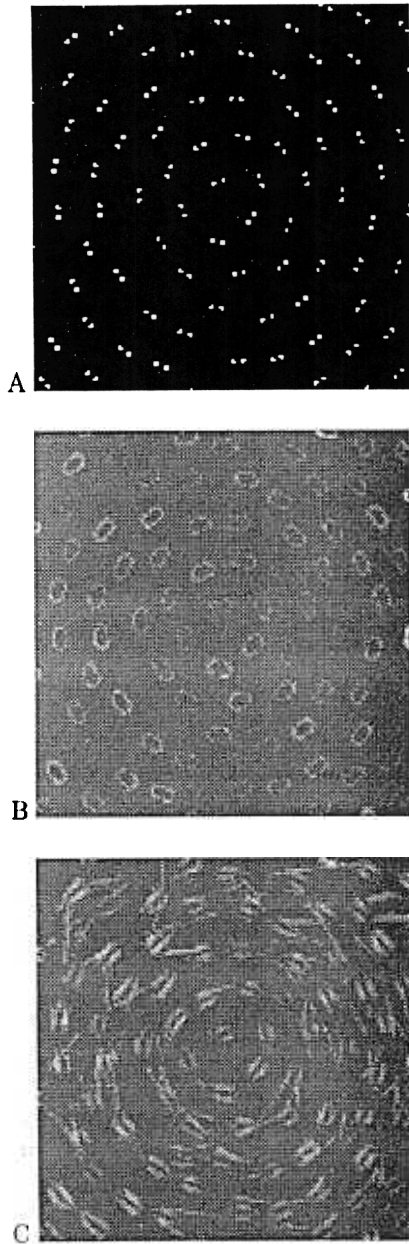


Fig. 13. Glass pattern. (A) The input image is a Stevens (1978) style Glass pattern. Note the circular organization characteristic of Glass patterns. (B) The complex cell stage output shown here in gray-scale format captures some of the circular impression. (C) The strong circular groupings become much more apparent after processing by the CC Loop, as seen in the equilibrium output of Competition 2.

opposite contrast polarities and are, in this sense, insensitive to contrast polarity, or direction-of-contrast. The theory predicts that boundaries are *seen* only if a filled-in brightness or color difference is generated on either side of the boundary positions within the surface representations of the FCS.

Boundaries may nonetheless be *recognized* by direct output signals from the BCS to an Object Recognition System (ORS) (Grossberg, 1987a, 1994; Grossberg & Mingolla, 1985b). Thus, one can “know” or “think about” a BCS input to the ORS even if the same BCS input to the FCS does not cause a difference in filled-in FCS activities that one can “see,” as in Fig. 1B. The

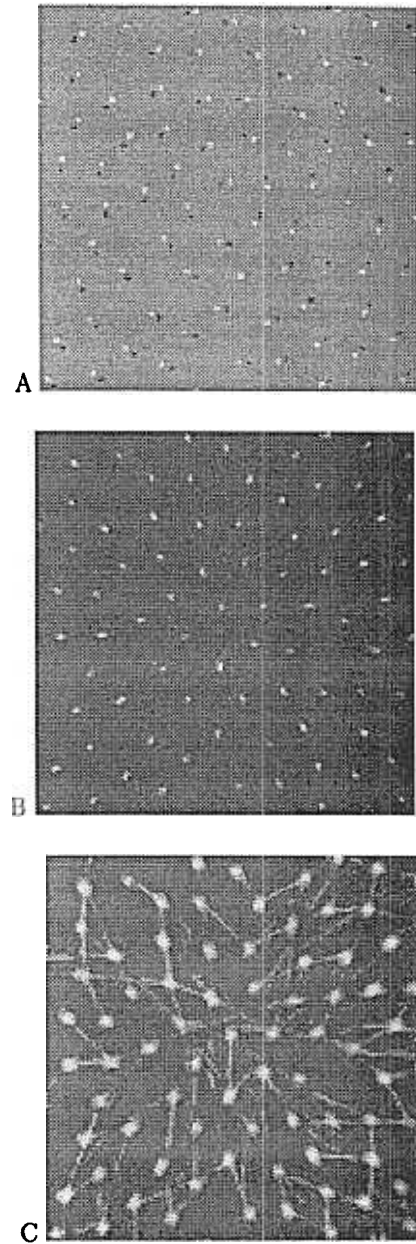


Fig. 14. Reverse contrast Glass pattern. (A) The input image is a reverse contrast Stevens-style Glass pattern. The circular organization is much less apparent in this case. (B) The OC Filter output shown here in gray-scale format does not give a circular impression at all, nor does the CC Loop output (C), which has completions that are predominately radial.

BCS signals to the ORS are interpreted to come from extrastriate cortical area V4 (Desimone et al., 1985; Zeki, 1983a,b) and the ORS is interpreted to include inferotemporal cortex (Mishkin, 1982; Mishkin & Appenzeller, 1987; Schwartz et al., 1983), among other areas. These proposed BCS ↔ ORS interactions are described in greater detail in Grossberg (1994) and Grossberg et al. (1994a).

Glass pattern simulations

The model's ability to generate boundary segmentations in response to statistically derived images is illustrated in Figs. 13

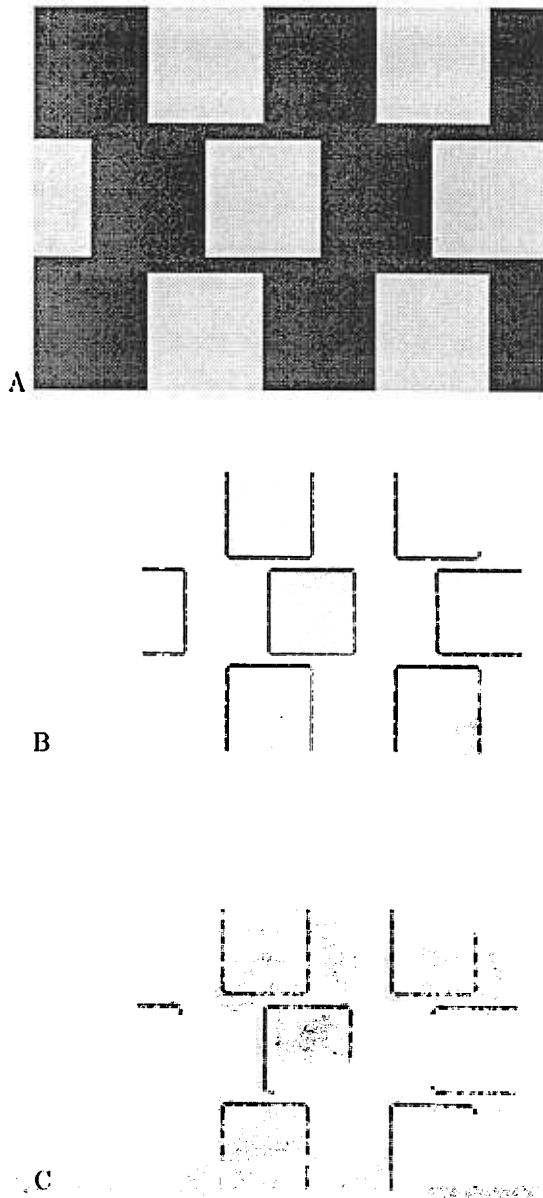


Fig. 15. (A) A small segment of the café wall image. (B) Complex cell responses to the segment are straight. (C) The CC Loop adds boundaries between the bricks, skewing them in the same directions as the perceptual effect.

and 14 with the Glass pattern and mixed-contrast Glass pattern simulations. A Glass pattern may be constructed by superimposing a slightly rotated copy of a random field of dots onto the original. For a large range of viewing distances, this gives the impression of a circular structure (Glass, 1969). The impression can be strengthened by placing the original dots on a randomly perturbed grid and setting a constant rotation distance, so that for every pair of corresponding dots, the distance between them is fixed (Stevens, 1978). This construction method was used to generate the Glass pattern input figure shown in Fig. 13A.

The model suggests that this percept is due to the combination of short-range correlations detected by the simple cells and long-range correlations detected by the bipole cells. Recall that simple cells are sensitive to contrast polarity. As a result, they

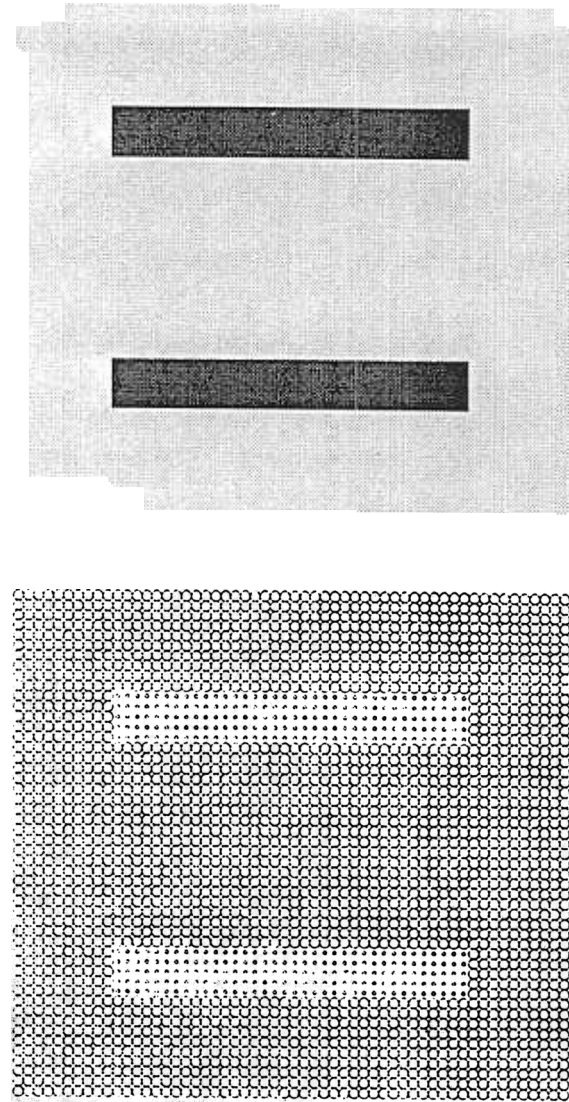


Fig. 16. The example input figure (above) is a 56 x 60 pixel image consisting of two low luminance bars on a high luminance background. The discrete representation (below) of the figure shows the magnitude of the simulated luminance at each pixel, as indicated by the size of each circle.

can preferentially respond to the pairs of dots in Fig. 13A, because the dots have the same contrast relative to the background. These colinear correlations are passed onto the complex cells (Fig. 13B). The complex cell responses are then passed through the hypercomplex cells before being linked together by bipole-hypercomplex cooperative-competitive feedback, the output of which is shown in Fig. 13C. Thus, although bipole cell receptive fields can pool image contrasts with opposite direction-of-contrast, their segmentations can become sensitive to direction-of-contrast through the prior action of simple cells.

The strong circular component of the boundary completions is both long-range and sharp. The oriented filtering is responsible for some of the circular appearance of the BCS boundaries, but the boundary completion definitely adds to the impression. To quantify this fact, the orientations of all of the nodes in the complex cell output were compared to the angle of the tangent

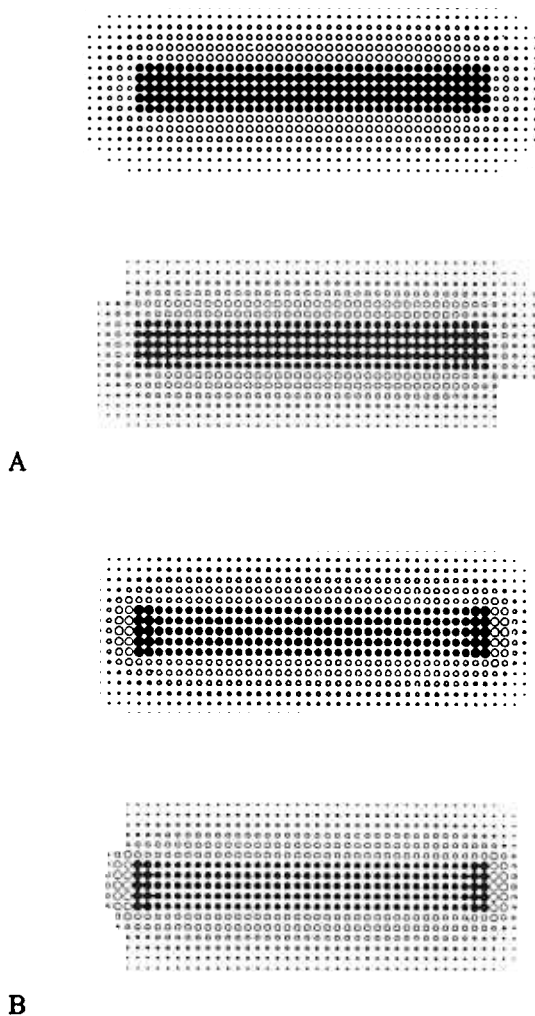


Fig. 17. Activation of the retinal and LGN networks. Unfilled circles represent the ON channel output; filled circles code the OFF response. Note the redistribution of activation in LGN (B) compared to the retinal pattern (A). The strongest signals in both the LGN ON and OFF channels are near the line end, whereas in the retinal stage output the strongest signals are found along the sides of the line.

at each node's location to a circle centered in the middle of the Glass pattern. If a node's activity is greater than 10% of the maximum activity and the node's orientation is within $\pi/8$ radians of the true tangent, then that node is considered "quasi-tangent." In the complex cell output (Fig. 13B), 27.9% of the nodes are quasi-tangent, as compared to 50.2% for the full BCS output (Fig. 13C). Thus, by the constructed measure, boundary completion contributes significantly to the circular appearance of the simulated Glass pattern.

In the mixed-contrast Glass pattern, dot pairs consist of one dot of positive contrast and a second of negative contrast relative to the background (Fig. 14A). The circular organization present in the original Glass pattern is much weaker in the reverse-contrast version. This is reflected in the model's complex cell (Fig. 14B) and hypercomplex cell (Fig. 14C) responses. The measure defined above quantifies this percept. In the complex cell output, 13.5% of the nodes are quasi-tangent. In the full BCS output, even fewer nodes, 4.0%, are quasi-tangent.

What makes the mixed-contrast Glass pattern percept different from the Glass pattern percept? The key model difference concerns the response of simple cells. Because model simple cells are sensitive to a definite direction-of-contrast, they are not optimally activated in a direction parallel to the dot-pair orientations of Fig. 14A. The bipole groupings are thus also different. This basic property of the model has been misunderstood by some investigators (e.g. Elder & Zucker, 1993), who have mistakenly inferred, because output cells of the BCS pool both directions-of-contrast, that BCS boundary segmentations are insensitive to image direction-of-contrast. Comparison of Figs. 13C and 14C shows that this is not correct.

Another difference between the simulations of like-contrast and mixed-contrast percepts is worth emphasizing. In Figs. 13 and 14, the switch to mixed image contrasts changes the boundary segmentation. In Figs. 11 and 12, it does not. Why is this? As noted in Grossberg and Mingolla (1985b), the difference lies in the simple cell response. In the case of the Glass pattern, the switch to mixed contrasts changes the orientations of the maximally activated simple cells from being colinear to the dot pairs towards being perpendicular to the bisector of the dot pairs. This difference in simple cell responses changes the long-range bipole-mediated boundary groupings from a circular to a radial tendency.

In the case of the Kanizsa square, the switch to mixed contrasts does not alter the orientations of maximally activated simple cells. Each pac man element of a Kanizsa square presents a consistent contour to the simple cells, whether its contrast is light-to-dark or dark-to-light. The bipole cells then generate a Kanizsa square in both cases by colinearly completing the pac man boundaries. In summary, the simple cell carries out a short-range grouping and the bipole cell a long-range grouping. The global patterning of contrasts in the image may or may not alter the way in which these two grouping scales interact. See Grossberg (1994) for other examples of this theme, particularly in explanations of how occluding and occluded contours, depth, and transparency interact.

The café wall illusion

Additional evidence that these short-range and long-range grouping mechanisms exist and interact as modeled can be seen in the café wall illusion. The café wall image (Fig. 15A) consists of only horizontal and vertical edges, yet it appears to have strong oblique components. The rectangle elements, or "bricks," appear to be trapezoids. The BCS simulation suggests that diagonal groupings between bricks are responsible for this percept. In the BCS output shown in Fig. 15C, the once horizontal complex cell boundaries of the central brick in Fig. 15B have been deformed so that the bricks now appears trapezoidal. A simulation on a smaller scale was presented in Grossberg and Mingolla (1985b). Morgan and Moulden (1986) have presented a similar explanation of this phenomenon.

Note that, in the café wall illusion, the simple and complex cells track the local image contrasts but the bipole cell groupings do not. For the mixed-contrast Glass pattern, the simple and complex cells do not track the local image contrasts and the bipole cell groupings follow suit. The café wall illusion hereby emphasizes that the long-range bipole grouping mechanism can generate nonveridical segmentations, even if its short-range inputs are veridical, in its effort to reconcile all of the statistical correlations that it senses on a larger spatial scale.

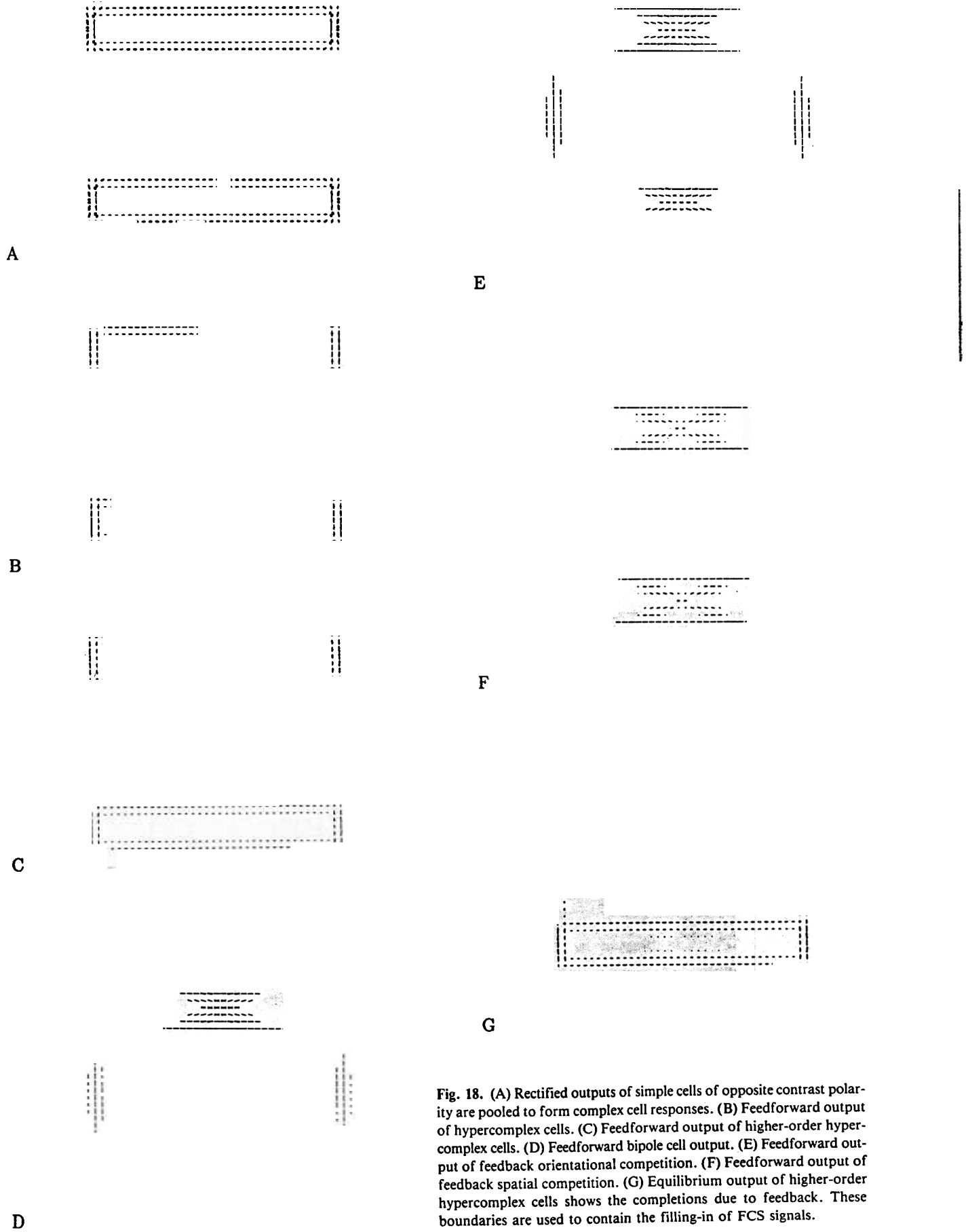


Fig. 18. (A) Rectified outputs of simple cells of opposite contrast polarity are pooled to form complex cell responses. (B) Feedforward output of hypercomplex cells. (C) Feedforward output of higher-order hypercomplex cells. (D) Feedforward bipole cell output. (E) Feedforward output of feedback orientational competition. (F) Feedforward output of feedback spatial competition. (G) Equilibrium output of higher-order hypercomplex cells shows the completions due to feedback. These boundaries are used to contain the filling-in of FCS signals.

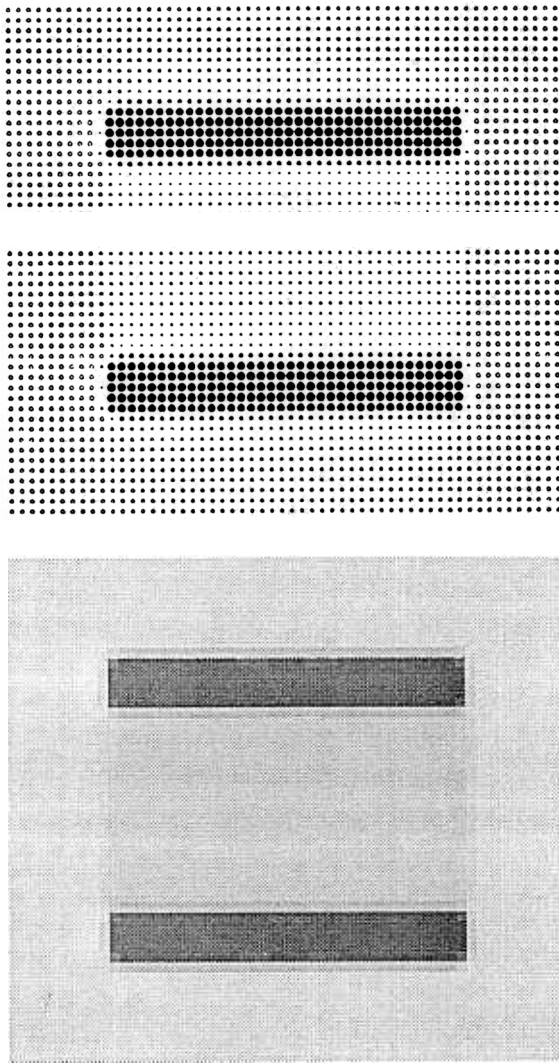


Fig. 19. The filled-in result which is the model analog of the visual percept. The result more closely resembles the visual percept when presented as a gray-scale image (below). Zero-valued nodes correspond to medium gray pixels in this image.

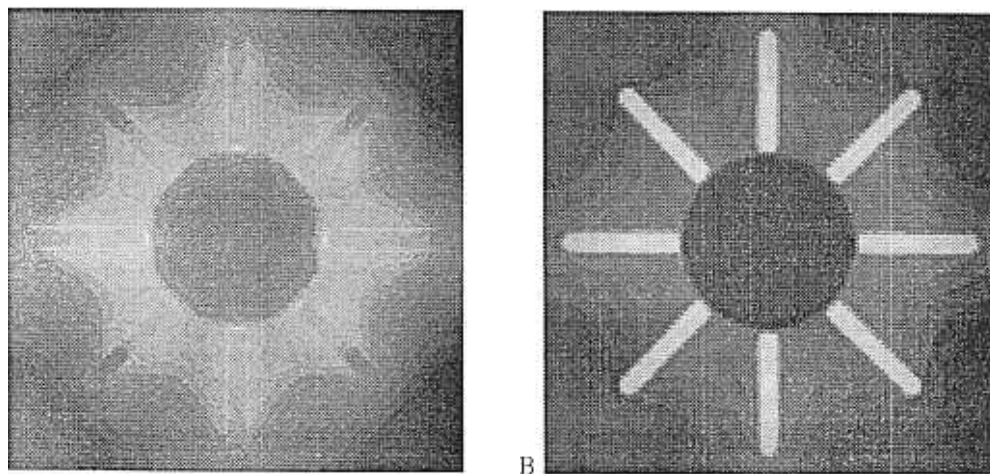


Fig. 20. The filled-in ON (A) and OFF (B) syncytia before being combined. Note that in (B), higher activity in the OFF channel is coded by brighter pixels, unlike the representation in Figs. 9–15 of net LGN activity.

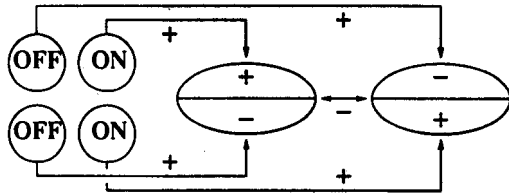
How do cortical simple cells respond preferentially to luminance discontinuities?

The mathematical equations that define the model depicted in Fig. 8 are given in the Appendix. This and the next section highlight two key features of the model to further clarify how its LGN and cortical mechanisms work together to simulate the above data properties.

The first feature concerns the design of cortical simple cells. How do simple cells integrate LGN signals from ON and OFF cells in such a way that true luminance discontinuities are favored, say, above ramps of equal net contrast? Fig. 21 depicts a model circuit in which ON cells turn on one-half of a simple cell receptive field and OFF cells turn on the other half. This is done for pairs of simple cells that are sensitive to opposite direction-of-contrast, or contrast polarity. Then the two cells inhibit one another before generating a rectified net output signal. This type of simple cell interaction has been reported experimentally (Ferster, 1988; Liu et al., 1992). The ON and OFF terms work together to ensure that simple cells favor regions between adjacent ON and OFF activity, where true luminance discontinuities occur. Although computing visual features such as edges is not a difficult problem in simple images, in processing complex images the combination of ON, OFF, and opponent inhibition plays a critical role in attenuating spurious image contrasts (Cruthirds et al., 1992; Grossberg et al., 1994*b*; Pessoa et al., 1994).

How does cortical cooperation generate curved illusory boundaries?

The next cortical feature worth emphasizing is the shape of the bipole cell receptive fields that carry out cooperative boundary completion. Model bipole cells have a pair of colinear oriented receptive fields that must both be activated to complete an intervening illusory contour. Bipole cells were predicted to exist in Cohen and Grossberg (1984) and Grossberg (1984) shortly before cortical cells with similar properties were reported by von der Heydt et al. (1984). At around the time of the von der Heydt et al. report, Grossberg and Mingolla (1985*a,b*) used bipole cell properties to simulate and explain a variety of data about illu-



0	1	0	0
0	1	0	0
		0	0
		+	0
		0	+

Fig. 21. Circuitry for LGN ON and OFF cell inputs to cortical simple cells. The table illustrates how ON, OFF, and inhibitory signals work together.

sory contour formation, neon color spreading, and texture segregation. Later reports extended this analysis to data sets about hyperacuity, shape-from-shading, depth perception, binocular rivalry, and the McCollough effect, among others (Grossberg, 1987a,b; Grossberg & Mingolla, 1987). This ever broadening explanatory range has allowed the accumulating weight of experimental evidence to refine model receptive fields, including bipole cell fields.

A persistent question about bipole cells has been: How can cells with such large and elongated receptive fields generate curved and sharp boundaries, such as those seen in all of the above simulations? The nonlinear cooperative-competitive feedback between hypercomplex cells and bipole cells controls boundary sharpness. Bipole receptive-field shape determines the ability to track curved boundaries.

The present version of the model uses a bipole filter whose receptive-field shape has properties consistent with Kellman and Shipley's (1991) "spatial relatability" condition. This condition constrains the circumstances under which boundary completion should be allowed to occur. Two boundaries are relatable, or can support a completion between them, when their extensions intersect in an obtuse or right angle. To see part of the motivation for this, consider two parallel line segments separated by a gap (Fig. 22). When the segments lie on the same line, the completion is straightforward. When the segments are offset, the extensions do not intersect. Thus the relatability condition is violated in this case. Note that the only possible smooth completion has an inflection point. The bottom of Fig. 22 also shows a case in which the segments are not parallel. These segments are relatable because their extensions do intersect an form an obtuse angle. Here the completion has no inflection point.

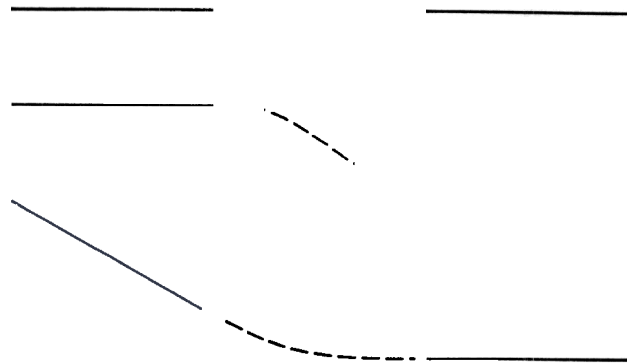


Fig. 22. The top and bottom images depict relatable contours, the middle case is not. See text for details.

Unlike the original bipole cell (e.g. Grossberg & Mingolla, 1985b) in which the optimal orientation for any filter location was radial (i.e. pointing toward the cell's origin), the optimal orientation for a point (p, q) in the new bipole filter is tangent to the circle C centered on the y -axis that passes through (p, q) and the origin $(0,0)$ of the receptive field (Fig. 23). Note that the circle is different for different filter locations. As in previous versions of the model, the actual filter values fall off exponentially as their orientations deviate from the optimal orientation determined by the tangent line. As seen in Fig. 23, the tangent line forms a larger angle than a line between (p, q) and the origin would, so that the new bipole receptive field satisfies the relatability condition most of the time. In certain circumstances, such as two parallel edges that are almost colinear, a completion can occur in the model that mathematically violates the Kellman and Shipley (1991) formulation of spatial relatability but is within a perceptually acceptable error range. That is, humans as well as the model at times perform completions that technically violate the relatability formula.

Filter values are further modulated by the slope of their tangent (small slopes are preferred to large slopes) and by their distance from the origin. A similar bipole filter with optimal orientations determined by parabolic equations was used to carry out BCS boundary segmentations of synthetic aperture radar images (Cruthirds et al., 1992). The overall shape of both filters is similar to the original bipole cell of Grossberg and Mingolla (1985b) and to the "association field" of Field et al. (1993).

After the bipole cells compute how much evidence for a boundary exists in each orientation, cells compete across orientation with other cells at the same position (see Fig. 8). This process selects the best orientation(s) for cells that receive cooperative feedback. Several orientations may be active at points receiving cooperative feedback. The competition selects at each position the best orientation, or orientations (at a corner), in order to produce completions that are as smooth as possible. This is especially important when the boundary being completed is not a straight contour, as occurs in the Ehrenstein figure (Figs. 1A and 9).

Concluding remarks

The neural model in this article suggests how reciprocal LGN-V1 and striate-extrastriate circuits may work together to generate emergent boundary segmentations and filled-in surface brightness properties that match a challenging set of psycho-

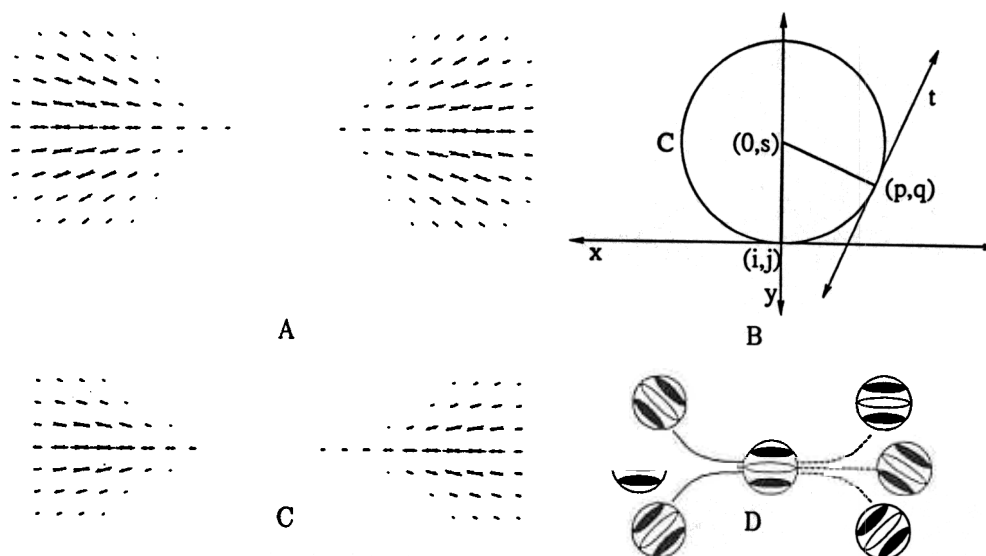


Fig. 23. (A) An example of a bipole "in-field" using the formula of Grossberg & Mingolla (1985b). The length of each segment is proportional to the "weight" afforded input to a bipole from a hypercomplex cell whose receptive-field center is at the center of the line segment and whose preferred orientation is that of the line segment. (B) In the present formulation, the optimal orientation for a bipole filter element at (p, q) is determined by the tangent t at that point to a circle C centered on the y -axis. See text for details. (C) An example of a bipole in-field generated according to the construction of (B). (D) The "association field" of Field et al. (1993) can be described by bipole interactions. Note that connections from the three Gabor filters on the left to the central one are denoted by solid lines, indicating that those combinations of preferred orientations support grouping, whereas connections from the central element to those on the right, denoted by broken lines, are between units of incompatible orientations, and therefore weak or absent. (Adapted with permission from Field et al., 1993).

physical data. The LGN-V1 circuit suggests how endstopped top-down $V1 \rightarrow$ LGN feedback can select LGN signals that are consistent with the tuning curves of their V1 targets, and thereby induce the brightness buttons that lead to perception of enhanced brightness in Ehrenstein disks. This enhancement also helps to synchronize the firing of LGN signals and to strengthen boundary signals at line ends.

Model cortical processing takes place in two parallel but interacting streams that simulate aspects of the parvocellular blob stream (FCS) and the interblob stream (BCS). The BCS models interactions between simple, complex, hypercomplex, higher-order hypercomplex, and bipole cells that communicate with each other *via* feedforward and feedback pathways. Previous articles (e.g. Francis et al., 1994; Grossberg, 1987b, 1994) have reviewed experimental evidence supporting the existence of each of these processing stages. Other studies have reviewed experimental evidence supporting the existence of FCS processes, particularly experiments about brightness, color, and depth perception and the temporal dynamics of filling-in (Arrington, 1994; Cohen & Grossberg, 1984; Grossberg, 1994; Grossberg & Todorović, 1988; Paradiso & Nakayama, 1991; Pessoa et al., 1995). In addition, the present model satisfies a test that few biologically derived models have heretofore passed: it works. The model has proven itself capable of processing complex imagery (Cruthirds et al., 1992; Grossberg et al., 1994b; Waxman et al., 1993), and thus has demonstrated the type of computational power that is needed to function in the real world.

Acknowledgments

Alan Gove's work was done while he was conducting doctoral research at Boston University and was supported under the Advanced Research

Projects Agency (AFOSR 90-0083). Stephen Grossberg was partially supported by the Air Force Office of Scientific Research (AFOSR F49620-92-J-0499), the Advanced Research Projects Agency (ONR N00014-92-J-4015), and the Office of Naval Research (ONR N00014-91-J-4100). Ennio Mingolla was partially funded by the Air Force Office of Scientific Research (AFOSR F49620-92-J-0334) and the Office of Naval Research (ONR N00014-91-J-4100 and ONR N00014-94-1-0597). The authors wish to thank Carol Y. Jefferson and Robin L. Locke for their valuable assistance in the preparation of the manuscript.

References

- ANDREOU, A.G. & BOAHEN, K.A. (1991). Modeling inner and outer plexiform retinal processing using nonlinear, coupled resistive networks. In *Human Vision, Visual Processing, and Digital Display II*, SPIE, 1453, pp. 270-281. Bellington, Washington: Society of Photo-Optical Instrumentation Engineers.
- ARRINGTON, K. (1994). The temporal dynamics of brightness filling-in. *Vision Research* 34, 3371-3387.
- CARPENTER, G.A. & GROSSBERG, S. (1991). *Pattern Recognition by Self-Organizing Neural Networks*. Cambridge, Massachusetts: MIT Press.
- CARPENTER, G.A. & GROSSBERG, S. (1993). Normal and amnesic learning, recognition, and memory by a neural model of cortico-hippocampal interactions. *Trends in Neurosciences* 16, 131-137.
- COHEN, M.A. & GROSSBERG, S. (1984). Neural dynamics of brightness perception: Features, boundaries, diffusion, and resonance. *Perception and Psychophysics* 36, 428-456.
- COREN, S. & HARLAND, R.E. (1993). Subjective contours and visual-geometric illusions: Do they share common mechanisms? *Italian Journal of Psychology* 20, 709-730.
- CRUTHIRDS, D.R., GOVE, A., GROSSBERG, S., MINGOLLA, E., NOWAK, N. & WILLIAMSON, J. (1992). Processing of synthetic aperture radar images by the Boundary Contour System and Feature Contour System. *Proceedings of the International Joint Conference on Neural Networks, IV*, pp. 414-419. Picataway, New Jersey: IEEE Service Center.
- DAUGMAN, J.G. (1980). Two-dimensional spectral analysis of cortical receptive field profiles. *Vision Research* 20, 847-856.

- DAY, R.H. & JORY, M.K. (1978). Subjective contours, visual acuity, and line contrast. In *Visual Psychophysics and Physiology*, ed. ARMINGTON, J.C., KRAUSKOPF, J.E. & WOOTEN, B., pp. 331-349. New York: Academic Press.
- DE YOE, E.A. & VAN ESSEN, D.C. (1988). Concurrent processing streams in monkey visual cortex. *Trends in Neuroscience* 11, 219-226.
- DESIMONE, R., SCHEIN, S.J., MORAN, J. & UNGERLEIDER, L.G. (1985). Contour, color, and shape analysis beyond the striate cortex. *Vision Research* 25, 441-452.
- DUBIN, M.W. & CLELAND, B.G. (1977). Organization of visual inputs to interneurons of lateral geniculate nucleus of the cat. *Journal of Neurophysiology* 40, 410-427.
- EHRENSTEIN, W. (1941). Über Abwandlungen der L. Hermannschen Heligkeitserscheinung. *Zeitschrift für Psychologie* 150, 83-91.
- ELDER, J. & ZUCKER, S. (1993). The effect of contour closure on the rapid discrimination of two-dimensional shapes. *Vision Research* 33, 981-991.
- EPSTEIN, W. (1993). On seeing that thinking is separate and on thinking that seeing is the same. *Italian Journal of Psychology* 20, 731-747.
- FERSTER, D. (1988). Spatially opponent excitation and inhibition in simple cells of the cat visual cortex. *Journal of Neuroscience* 8, 1172-1180.
- FIELD, D.J., HAYES, A. & HESS, R.F. (1993). Contour integration by the human visual system: Evidence for a local "association field." *Vision Research* 33, 173-193.
- FRANCIS, G. & GROSSBERG, S. (1994). Cortical dynamics of form and motion integration: Persistence, apparent motion, and illusory contours. Technical Report CAS/CNS-TR-94-011, Boston, MA: Boston University. *Vision Research* (in press).
- FRANCIS, G. & GROSSBERG, S. (1995). Cortical dynamics of boundary segmentation and reset: Persistence, afterimages, and residual traces (Technical Report CAS/CNS-TR-95-002). *Perception* (in press).
- FRANCIS, G., GROSSBERG, S. & MINGOLLA, E. (1994). Cortical dynamics of feature binding and reset: Control of visual persistence. *Vision Research* 34, 1089-1104.
- FRISBY, J.P. & CLATWORTHY, J.L. (1975). Illusory contours: Curious cases of simultaneous brightness contrast? *Perception* 4, 349-357.
- FUNKE, K. & EYSEL, U.T. (1992). EEG-dependent modulation of response dynamics of cat dLGN relay cells and the contribution of corticogeniculate feedback. *Brain Research* 573, 217-227.
- GILBERT, C.D. & KELLY, J.P. (1975). The projections of cells in different layers of the cat's visual cortex. *Journal of Comparative Neurology* 163, 81-106.
- GILLAM, B.J. & GOODENOUGH, B. (1994). Subjective contours at line terminators—The effect of the relationship between terminator arrangement and line arrangement. *Investigative Ophthalmology and Visual Science* 35, 1627.
- GLASS, L. (1969). Moiré effect from random dots. *Nature* 223, 578-580.
- GOVE, A.N., GROSSBERG, S. & MINGOLLA, E. (1994). A link between brightness perception, illusory contours, and binocular corticogeniculate feedback. *Investigative Ophthalmology and Visual Science* 35, 1437.
- GREGORY, R.L. (1993). Seeing and thinking. *Italian Journal of Psychology* 20, 749-769.
- GROSSBERG, S. (1976). Adaptive pattern classification and universal recoding, II: Feedback, expectation, olfaction, and illusions. *Biological Cybernetics* 23, 187-202.
- GROSSBERG, S. (1980). How does a brain build a cognitive code? *Psychological Review* 87, 1-51.
- GROSSBERG, S. (1983). The quantized geometry of visual space: The coherent computation of depth, form, and lightness. *Behavioral and Brain Sciences* 6, 625-657.
- GROSSBERG, S. (1984). Outline of a theory of brightness, color, and form perception. In *Trends in Mathematical Psychology*, ed. DEGREEF, E. & VAN BUGGENHAUT, J., pp. 59-86. Amsterdam: Elsevier/North-Holland.
- GROSSBERG, S. (1987a). Cortical dynamics of three-dimensional form, color, and brightness perception, I: Monocular theory. *Perception and Psychophysics* 41, 87-116.
- GROSSBERG, S. (1987b). Cortical dynamics of three-dimensional form, color, and brightness perception, II: Binocular theory. *Perception and Psychophysics* 41, 117-158.
- GROSSBERG, S. (1994). 3-D vision and figure-ground separation by visual cortex. *Perception and Psychophysics* 55, 48-120.
- GROSSBERG, S. & MINGOLLA, E. (1985a). Neural dynamics of form perception: Boundary completion, illusory figures, and neon color spreading. *Psychological Review* 92, 173-211.
- GROSSBERG, S. & MINGOLLA, E. (1985b). Neural dynamics of perceptual grouping: Textures, boundaries, and emergent segmentations. *Perception and Psychophysics* 38, 141-171.
- GROSSBERG, S. & MINGOLLA, E. (1987). Neural dynamics of surface perception: Boundary webs, illuminants, and shape-from-shading. *Computer Vision, Graphics, and Image Processing* 37, 116-165.
- GROSSBERG, S., MINGOLLA, E. & ROSS, W.D. (1994a). A neural theory of attentive visual search: Interactions of boundary, surface, spatial, and object representations. *Psychological Review* 101, 470-489.
- GROSSBERG, S., MINGOLLA, E. & WILLIAMSON, J. (1994b). Synthetic aperture radar processing by a multiple scale neural system for boundary and surface representation. Technical Report CAS/CNS-TR-94-001, Boston, MA: Boston University. *Neural Networks* (in press).
- GROSSBERG, S., MINGOLLA, E. & TODOROVIĆ, D. (1989). A neural network architecture for preattentive vision. *IEEE Transactions on Bio-medical Engineering* 36, 65-83.
- GROSSBERG, S. & TODOROVIĆ, D. (1988). Neural dynamics of 1-D and 2-D brightness perception: A unified model of classical and recent phenomena. *Perception and Psychophysics* 43, 241-277.
- GROSSBERG, S. & WYSE, L. (1991). A neural network architecture for figure-ground separation of connected scenic figures. *Neural Networks* 4, 723-742.
- GUILLERY, R.W. (1967). Patterns of fiber degeneration in the dorsal lateral geniculate nucleus of the cat following lesions in the visual cortex. *Journal of Comparative Neurology* 130, 197-222.
- HALPERN, D.F. (1981). The determinants of illusory-contour perception. *Perception* 10, 199-213.
- HUBEL, D.H. & WIESEL, T.N. (1977). Functional architecture of macaque monkey visual cortex. *Proceedings of the Royal Society B (London)* 198, 1-59.
- HULL, D.H. (1968). Corticofugal influence in the macaque lateral geniculate nucleus of the cat. *Vision Research* 8, 1285-1298.
- KALLI, R.E. & CHASE, R. (1970). Corticofugal influence on activity of lateral geniculate nucleus neurons in the cat. *Journal of Neurophysiology* 33, 459-474.
- KANIZSA, G. (1979). *Organization in Vision*. New York: Praeger Publishing.
- KELLMAN, P.J. & SHIPLEY, T.F. (1991). A theory of interpolation in object perception. *Cognitive Psychology* 23, 141-221.
- KENNEDY, J.M. (1979). Subjective contours, contrast, and assimilation. In *Perception and Pictorial Representation*, ed. NODINE, C.F. & FISHER, D.F., New York: Praeger.
- KENNEDY, J.M. (1988). Line endings and subjective contours. *Spatial Vision* 3, 151-158.
- KOCH, C. (1987). The action of the corticofugal pathway on sensory thalamic nuclei: A hypothesis. *Neuroscience* 23, 399-406.
- LESHER, G.W. Illusory contours: Toward a neurally based perceptual theory. *Psychological Bulletin* (in press).
- LIU, Z., GASKA, J.P., JACOBSON, L.D. & POLLEN, D.A. (1992). Inter-neuronal interaction between members of quadrature phase and anti-phase pairs in the cat's visual cortex. *Vision Research* 32, 1193-1198.
- MARČELJA, S. (1980). Mathematical description of the responses of simple cortical cells. *Journal of the Optical Society of America* 70, 1297-1300.
- MARROCCO, R.T. & McCLURKIN, J.W. (1985). Evidence for spatial structure in cortical input to the monkey lateral geniculate nucleus. *Experimental Brain Research* 59, 50-56.
- MICHOTTE, A., THINES, G. & CRABBE, G. (1964). *Les compléments amodaux des structures perceptives*. Louvain: Publications Universitaires de Louvain.
- MISHKIN, M. (1982). A memory system in the monkey. *Philosophical Transactions Royal Society B (London)* 298, 85-95.
- MISHKIN, M. & APPENZELLER, T. (1987). The anatomy of memory. *Scientific American* 256, 80-89.
- MONTERO, V.M. (1990). Quantitative immunogold analysis reveals high glutamate levels in synaptic terminals of retino-geniculate corticogeniculate, and geniculo-cortical axons in the cat. *Visual Neuroscience* 4, 437-443.
- MONTERO, V.M. & ZEMPEL, J. (1985). Evidence for two types of GABA-containing interneurons in the A-laminae of the cat lateral geniculate nucleus: A double-label HRP and GABA-immunocytochemical study. *Experimental Brain Research* 60, 603-609.

- MORGAN, M.J. & MOULDEN, B. (1986). The Münsterberg figure and twisted cords. *Vision Research* 26, 1793–1800.
- MURPHY, P.C. & SILLITO, A.M. (1987). Corticofugal influences on the generation of length tuning in the visual pathway. *Nature* 329, 727–729.
- PARADISO, M. & NAKAYAMA, K. (1991). Brightness perception and filling-in. *Vision Research* 31, 1221–1236.
- PESSOA, L., MINGOLLA, E. & NEUMANN, H. (1995). A contrast- and luminance-driven multiscale network model of brightness perception. *Visual Research* 35, 2201–2233.
- PETZOLD, L.R. (1983). Automatic selection of methods for solving stiff and non-stiff systems of ordinary differential equations. *SIAM Journal of Scientific and Statistical Computing* 4, 136–148.
- POLLEN, D.A. & RONNER, S.F. (1981). Phase relationships between adjacent simple cells in the visual cortex. *Science* 212, 1409–1411.
- REDIES, C., CROOK, J.M. & CREUTZFELDT, O.D. (1986). Neuronal responses to borders with and without luminance gradients in cat visual cortex and dLGN. *Experimental Brain Research* 61, 469–481.
- ROBSON, J.A. (1983). The morphology of corticofugal axons to the dorsal lateral geniculate nucleus in the cat. *Journal of Comparative Neurology* 216, 89–103.
- SCHILLER, P. (1992). The ON and OFF channels of the visual system. *Trends in Neuroscience* 15, 86–92.
- SCHWARTZ, E.L., DESIMONE, R., ALBRIGHT, T. & GROSS, C.G. (1983). Shape recognition and inferior temporal neurons. *Proceedings of the National Academy of Sciences of the U.S.A.* 80, 5776–5778.
- SILLITO, A.M., JONES, H.E., GERSTEIN, G.L. & WEST, D.C. (1994). Feature-linked synchronization of thalamic relay cell firing induced by feedback from the visual cortex. *Nature* 369, 479–482.
- SILLITO, A.M. & KEMP, J.A. (1983). The influence of GABAergic inhibitory processes on the receptive field structure of X and Y cells in cat dorsal lateral geniculate nucleus (dLGN). *Brain Research* 277, 63–77.
- SINGER, W. (1977). Control of thalamic transmission by corticofugal and ascending reticular pathways in the visual system. *Physiological Review* 57, 386–420.
- SINGER, W. (1979). Central-core control of visual-cortex functions. In *Neurosciences Fourth Study Program*, ed. SCHMITT, F.O. et al., Cambridge, Massachusetts: M.I.T. Press.
- SPITZER, H. & HOCHSTEIN, S. (1985). A complex-cell receptive field model. *Journal of Neurophysiology* 33, 1266–1286.
- STEVENS, K.A. (1978). Computation of locally parallel structure. *Biological Cybernetics* 29, 19–28.
- UPDYKE, B.V. (1975). The patterns of projection of cortical areas 17, 18, and 19 onto the laminae of the dLGN in the cat. *Journal of Comparative Neurology* 163, 377–396.
- VARELA, F.J. & SINGER, W. (1987). Neuronal dynamics in the visual corticothalamic pathway revealed through binocular rivalry. *Experimental Brain Research* 66, 10–20.
- VON DER HEYDT, R., PETERHANS, E. & BAUMGARTNER, G. (1984). Illusory contours and cortical neuron responses. *Science* 224, 1260–1262.
- WATANABE, T. & SATO, T. (1989). Effects of luminance contrast on color spreading and illusory contour in the neon color spreading effect. *Perception and Psychophysics* 45, 427–430.
- WATANABE, T. & TAKEICHI, H. (1990). The relation between color spreading and illusory contours. *Perception and Psychophysics* 47, 457–467.
- WAXMAN, A.M., SEIBERT, M., BERNARDON, A.M. & FAY, D.A. (1993). Neural systems for automatic target learning and recognition. *The Lincoln Laboratory Journal* 6, 77–116.
- WEBER, A.J., KALIL, R.E. & BEHAN, M. (1989). Synaptic connections between corticogeniculate axons and interneurons in the dorsal lateral geniculate nucleus of the cat. *Journal of Comparative Neurology* 289, 156–164.
- ZEKI. (1983a). Colour coding in the cerebral cortex: The reaction of cells in monkey visual cortex to wavelengths and colours. *Neuroscience* 9, 741–765.
- ZEKI. (1983b). Colour coding in the cerebral cortex: The responses of wavelength-selective and colour coded cells in monkey visual cortex to changes in wavelength composition. *Neuroscience* 9, 767–791.

Appendix: An improved neural model of boundary completion and surface filling-in

This section describes the revised BCS and FCS equations after incorporation of the enhancements and revisions discussed in

the text. Additional modifications from equations employed for previously published simulations are also included, including ON and OFF LGN cells, and improved cortical bipole cell receptive fields and hypercomplex-bipole feedback interactions (Cruthirds et al., 1992; Grossberg & Wyse, 1991). The structure of the improved model, as shown in Fig. 8, includes an OFF channel, an LGN stage, and feedback from the cortex to the LGN stage.

In addition to the mathematical description of each stage, convolution filters are displayed graphically, and the output of each stage is shown for an image of sufficient simplicity to allow a detailed inspection of the effects of each stage (Fig. 16). Parameter values are also listed for each stage. These values are used for all the simulations in this article.

ON and OFF retinal shunting networks

This first stage of processing involves two parallel center-surround networks. These networks compensate for variable illumination (“discount the illuminant”) while suppressing noise and computing contrasts in the image. In the ON channel, the center is excitatory while the surround is inhibitory (Fig. 24A), whereas in the OFF channel, the center is inhibitory and the surround is excitatory (Fig. 24B). The cells in each channel obey membrane, or shunting, equations coupled by distance-dependent interactions (Grossberg, 1983), whereby inputs I_{pq} at position (p, q) are filtered by convolution filters that are defined by isotropic two-dimensional Gaussians. The ON and OFF channels thus have activities x_{ij}^+ and x_{ij}^- , respectively, at cell positions (i, j) that satisfy the following equations:

On retinal cells

$$\begin{aligned} \frac{d}{dt} x_{ij}^+ = & -Dx_{ij}^+ + (U - x_{ij}^+) \sum_{p,q} C_{pqij} I_{pq} \\ & - (x_{ij}^+ + L) \sum_{p,q} S_{pqij} I_{pq} \end{aligned} \quad (1)$$

and

OFF retinal cells

$$\begin{aligned} \frac{d}{dt} x_{ij}^- = & -Dx_{ij}^- + (U - x_{ij}^-) \sum_{p,q} S_{pqij} I_{pq} \\ & - (x_{ij}^- + L) \sum_{p,q} C_{pqij} I_{pq} \end{aligned} \quad (2)$$

where U and L are the upper and lower bounds of the activities x^+ and x^- ,

$$C_{pqij} = Cg_2(p, q, i, j, \sigma_c), \quad S_{pqij} = Sg_2(p, q, i, j, \sigma_s) \quad (3)$$

and the two-dimensional Gaussian function g_2 is defined as

$$g_2(p, q, i, j, \sigma) = \frac{1}{2\pi\sigma^2} \exp\left\{-\frac{1}{2\sigma^2} ((p-i)^2 + (q-j)^2)\right\} \quad (4)$$

At equilibrium the ON channel activity is defined by

$$x_{ij}^+ = \frac{\sum_{p,q} (UC_{pqij} - LS_{pqij}) I_{pq}}{D + \sum_{p,q} (C_{pqij} + S_{pqij}) I_{pq}} \quad (5)$$

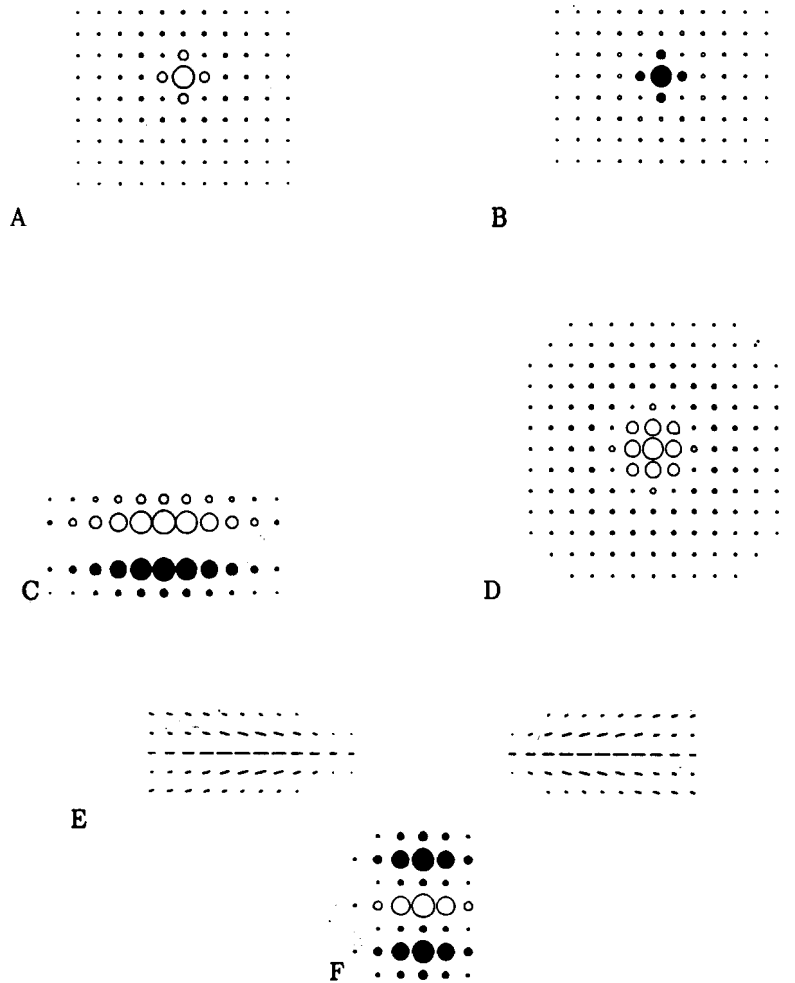


Fig. 24. DOG filters for the ON (A) and OFF (B) channel retinal output cell. Unfilled circles code positive values, filled circles represent negative values. Both filters have a 3-by-3 center and a 15-by-15 surround. (C) Discrete Gabor filter for a horizontal simple cell. (D) Filter for Competition 1. (E) Cooperative bipole filter. (F) Filter for Competition 1F.

and the OFF channel activity is defined by

$$x_{ij}^- = \frac{\sum_{p,q} (US_{pqij} - LC_{pqij}) I_{pq}}{D + \sum_{p,q} (C_{pqij} + S_{pqij}) I_{pq}} \quad (6)$$

A threshold-linear, or half-wave rectified, output function $T(x)$ is applied to the ON and OFF activities of this stage, where

$$T(x) = \max(0, x) \quad (7)$$

This function is also used in other stages.

The input image (Fig. 16) consists of two parallel bars of low luminance on a high luminance background. The output of the retinal stage is shown in Fig. 17A. The parameter values for eqns. (2)–(4) are $D = 1$, $U = 1$, $L = 1$, $\sigma_c = 0.58$, and $\sigma_s = 2.90$. As a result, $x_{ij}^+ + x_{ij}^- = 0$. Therefore, it is possible to display both outputs in a single image. In Fig. 17A, open circles key ON channel values, and filled circles key OFF channel values. As illustrated in Fig. 2, the ON channel responds near the outside of the bars, and the OFF channel cells respond to the interior of the bars. Far from the bars the input pattern is uniform, so neither channel responds.

The parameters C and S in eqn. (3) were chosen so that when the two Gaussian functions are combined into a DOG filter, the positive- and negative-valued filter elements both have an absolute sum of 1. Thus $C = 1.19$ and $S = 1.20$. The input image I in this simulation has values in the range $[0, 1]$. The interior regions of the bars have pixel value 0.1, while the background pixels all have value 1.0.

LGN circuit

In the model, LGN relay cells r receive excitatory signals T from retina, excitatory signals E from cortical endstopped cells and inhibitory signals M from LGN interneurons, which are also activated by feedback. The model equations for ON and OFF relay cells are given by

LGN ON relay cells

$$\begin{aligned} \frac{d}{dt} r_{ij}^+ = & -Dr_{ij}^+ + (U - r_{ij}^+) \left[T(x_{ij}^+) + T(x_{ij}^+) \sum_{p,q} C_{pqij} E_{pq} \right] \\ & - (r_{ij}^+ + L) \sum_{p,q} S_{pqij} M_{pq} \end{aligned} \quad (8)$$

and

LGN OFF relay cells

$$\frac{d}{dt} r_{ij}^- = -Dr_{ij}^- + (U - r_{ij}^-) \left[T(x_{ij}^-) + T(x_{ij}^-) \sum_{p,q} C_{pqij} E_{pq} \right] - (r_{ij}^- + L) \sum_{p,q} S_{pqij} M_{pq} \quad (9)$$

where $C_{pqij} = Cg_2(p, q, i, j, \sigma_c)$ and $S_{pqij} = Sg_2(p, q, i, j, \sigma_s)$ are on-center and off-surround Gaussian kernels, respectively, and U and L are the upper and lower bounds, respectively, of r 's activity. The feedback to this stage is computed by summing over orientation the activity of cortical cells from the outputs E of endstopped hypercomplex cells:

$$E_{ij} = T\left(\sum_k w_{ijk} - W\right) \quad (10)$$

The activity of w_{ijk} is defined by eqns. (21)–(24). The inter-neuron activity M is similarly defined by

$$M_{ij} = T\left(\sum_k w_{ijk} - W\right) \quad (11)$$

Note that in the excitatory terms of eqns. (8) and (9) the feedback is gated by the bottom-up signal x_{ij} . As a result, the feedback can only enhance the activity of cells that already receive retinal input. In the inhibitory terms the feedback does not interact with the bottom-up input. Both terms are consistent with the discussion of LGN circuitry in cat by Weber et al. (1989). Although bottom-up retinal input, by itself, can activate model LGN cells, top-down corticogeniculate feedback cannot, by itself, activate model LGN cells. When both bottom-up and top-down inputs are active, a match between bottom-up retinal input with top-down cortical input can enhance LGN processing, while LGN processing of bottom-up retinal inputs that have no top-down support is suppressed.

The result of processing the bar image with the LGN stage is shown in Fig. 17B. The output LGN output has stronger signals at the ends of the bars rather than at its sides. These are the model analog of brightness buttons.

By eqns. (8) and (9), at equilibrium, the ON and OFF cell activities of the LGN stage obey the equations

$$r_{ij}^+ = \frac{UT(x_{ij}^+) + UT(x_{ij}^+) \sum_{p,q} C_{pqij} E_{pq} - L \sum_{p,q} S_{pqij} M_{pq}}{D + T(x_{ij}^+) + T(x_{ij}^+) \sum_{p,q} C_{pqij} E_{pq} + \sum_{p,q} S_{pqij} M_{pq}} \quad (12)$$

and

$$r_{ij}^- = \frac{UT(x_{ij}^-) + UT(x_{ij}^-) \sum_{p,q} C_{pqij} E_{pq} - L \sum_{p,q} S_{pqij} M_{pq}}{D + T(x_{ij}^-) + T(x_{ij}^-) \sum_{p,q} C_{pqij} E_{pq} + \sum_{p,q} S_{pqij} M_{pq}} \quad (13)$$

Default parameters for eqns. (12) and (13) of the LGN stage are $D = 1$, $U = 1$, $L = 1$, $C = 100$, $\sigma_c = 1.0$, $S = 10$, $\sigma_s = 3.0$, $W = 0.16$. (Subscripts on parameters such as U , L , C , and S are omitted in their several uses for simplicity.)

Simple and complex cell layers

The oriented cells used here are odd-symmetric Gabor filters (Daugman, 1980; Marčelja, 1980). Including even Gabor cells may improve the system's boundary detection capabilities (Cruthirds et al., 1992; Pollen & Ronner, 1981; Spitzer & Hochstein, 1985), but adequate results were here obtained without them.

Each odd cell has two subregions, A and B , that are symmetric about the cell's long axis (Fig. 24C). Region A is excited by net ON channel signals while region B is excited by net OFF channel signals. For each of the K discrete orientations used in the model, there are two simple cells of opposite polarity. Thus there are $2K$ simple cells, whose activities are half-wave rectified and combined pairwise to activate K complex cells (Grossberg & Mingolla, 1985b).

Each simple cell subregion computes the net ON minus OFF (or OFF minus ON) response for the entire subregion:

$$A_{ijk} = \sum_{p,q} (T(r_{ij}^+) - T(r_{pq}^-)) T(G_{pqij}^{(k)}) \quad (14)$$

and

$$B_{ijk} = \sum_{p,q} (T(r_{pq}^-) - T(r_{pq}^+)) T(-G_{pqij}^{(k)}) \quad (15)$$

where the oriented Gabor filters $G_{pqij}^{(k)}$, with orientation k , are rotated versions of the horizontal filter with orientation $k = 0$ and frequency ω , that is defined by

$$G_{pqij}^{(0)} = G \sin(2\pi\omega(q - j)) \exp\left\{-\frac{1}{2}\left(\left(\frac{p - i}{\sigma_h}\right)^2 + \left(\frac{q - j}{\sigma_v}\right)^2\right)\right\} \quad (16)$$

For this and all anisotropic filters used in the model, the equation for the horizontal filter is given. Computation of filter orientations other than horizontal is done by first rotating the filter plane to align the filter's long axis with the x -axis, and then calculating each filter value by applying the equation for the horizontal filter. For a filter with orientation index k , for example, location (p, q) is first rotated by $\theta_k = -k\pi/K$ to give new coordinates (p', q') defined by

$$p' = p \cos(\theta_k) - q \sin(\theta_k) \quad (17)$$

and

$$q' = p \sin(\theta_k) + q \cos(\theta_k) \quad (18)$$

Then the equation for the horizontal filter at (p, q) is applied to (p', q') . In this way, filter values are computed for filters of every orientation.

The simple cell receptive field is designed so that its activity s_{ijk} is largest when a correctly oriented net ON signal occurs in one half of the cell's receptive field and on equal net OFF signal occurs in the other half. This property is captured by the equation

Simple cells

$$s_{ijk} = T(A_{ijk} + B_{ijk} - \alpha|A_{ijk} - B_{ijk}|) \quad (19)$$

The first two terms compute the net ON and OFF activity of the two subregions, which can be positive or negative. The sum

$A_{ijk} + B_{ijk}$ in eqn. (19) can be interpreted as the net effect of two operations. In the first operation, ON cells turn on one-half of a simple cell's receptive field, as in term $T(r_{pq}^+)G_{pqij}^{(k)}$, and OFF cells turn on the other half, as in term $T(r_{ij}^-)t(-G_{pqij}^{(k)})$. This is done for pairs of simple cells that are sensitive to opposite direction-of-contrast. Then the two cells inhibit one another before generating a net output signal, as diagrammed in Fig. 21. The remaining term $-\alpha|A_{ijk} - B_{ijk}|$ in eqn. (19) reduces the simple cell response when the subregions are not equally activated, with the parameter α determining the strength of the "penalty." These terms work together to ensure that simple cells favor regions between adjacent ON and OFF activity, where true luminance discontinuities typically occur.

The complex cell activity c_{ijk} is the sum of half-wave rectified signals from pairs of like-oriented simple cells of opposite contrast-polarity:

Complex cells

$$c_{ijk} = s_{ijk} + s_{ij(k+K)} \quad \text{for } 0 \leq k < K \quad (20)$$

The original simple and complex cell layer equation in Grossberg and Mingolla (1985a) combined area normalization (in the denominator) with oriented filtering. Because the input to the new version is already normalized with respect to area by the retinal stage, normalization is not needed here, and is omitted for simplicity.

Parameter values for the simple cell stage are $\omega = 0.2$, $\sigma_h = 1.833$, $\sigma_v = 0.833$, $\alpha = 1.3$, and $K = 12$. Parameter G in eqn. (16) was chosen so that the absolute sum of the positive and of the negative values in the Gabor filter is 1. Because of pixel sampling differences for different orientations, the value of G varied slightly with orientation. In the horizontal ($k = 0$) case, $G = 0.556$. The output of the complex cell layer for the two-bar simulation is shown in Fig. 18A.

Hypercomplex cells: Spatial competition

This stage uses competition across space, or an endstopping operation, among like-oriented cells to convert output signals from model complex cells into input signals to the first population of model hypercomplex cells, which is called the first competitive stage, or Competition 1. The output of the first competitive stage is used as feedback to the LGN stage, as in eqns. (10) and (11), as well as input to the higher-order hypercomplex cells. Competition 1 takes the form of a standard shunting equation, with two additional terms, a tonic input J and feedback v that derives from a later stage in the cooperative-competitive grouping network, or CC Loop:

$$\frac{d}{dt} w_{ijk} = -Dw_{ijk} + (U - w_{ijk}) \left(\sum_{p,q} C_{pqij} c_{pqk} + FT(v_{ijk}) + J \right) - (w_{ijk} + L) \sum_{p,q,r} S_{pqij}^{(r,k)} c_{pqr} \quad (21)$$

The excitatory convolution filter is a two-dimensional Gaussian across space:

$$C_{pqij} = Cg_2(p, q, i, j, \sigma_c) \quad (22)$$

while the inhibitory convolution filter includes nearby orientations as well:

$$S_{pqij}^{(r,k)} = Sg_2(p, q, i, j, \sigma_s) g_1(r, k, \sigma_r) \quad (23)$$

where g_1 is a one-dimensional Gaussian

$$g_1(r, k, \sigma) = (2\pi\sigma^2)^{-1/2} \exp\left\{-\frac{1}{2\sigma^2}(r - k)^2\right\}$$

(see Fig. 24D). This form of inhibition prevents non-dominant orientations from producing undesired effects. In particular, if competition were strictly among cells of identical orientations, then cells of the preferred orientation in a given region could inhibit one another, while a single, or small number, of "noise" cells of a nearby orientation could have its activity (relatively) enhanced for lack of competitors. At equilibrium, the activities of the first competitive stage are thus defined by

$$w_{ijk} = \frac{UJ + UFT(v_{ijk}) + U \sum_{p,q} C_{pqij} c_{pqk} - L \sum_{p,q,r} S_{pqij}^{(r,k)} c_{pqr}}{D + J + FT(v_{ijk}) + \sum_{p,q} C_{pqij} c_{pqk} + \sum_{p,q,r} S_{pqij}^{(r,k)} c_{pqr}} \quad (25)$$

which generalizes the first competitive stage of Grossberg and Mingolla (1987). As in that model, the difference of Gaussians term in the numerator of eqn. (25) intensifies the competition between nearby cells of the same orientation so that it is possible to drive a losing cell's activity down to zero. When the input to the competition has boundaries that are several pixels wide, the thickness of the boundaries can be reduced to one or two pixels.

As in Grossberg and Mingolla (1985b, 1987), this stage also performs endstopping. The convolution filter has a center-surround structure so that a line that fits within the central region will produce a stronger response than a line that also extends into the surround. Because the input to this stage is oriented, the isotropic convolution filter can appear to favor lines of a certain length at a specific orientation. The enhancement of the line ends (and the relative weakening of the line sides) can be seen in the output of this stage (Fig. 18B). Parameter values for eqn. (25) are $D = 1$, $U = 1$, $L = 1$, $J = 0.01$, and $F = 0.03$. Filter parameters in eqns. (22) and (23) are $C = 1.0$, $\sigma_c = 1.0$, $S = 1.0$, $\sigma_s = 3.5$, and $\sigma_r = 2.0$.

Higher-order hypercomplex cells: Orientational competition

This competition takes place across the orientation dimension. At each spatial position, cells compete with other cells that have same position but different orientation. The result is orientational sharpening at image locations where no single orientation is the clear winner. The other effect of this stage is disinhibition of signals perpendicular to those that were inhibited below the tonic level J in Competition 1. This can cause new signals to appear that flank and are perpendicular to existing boundaries. These new endcut signals help to generate boundaries, such as the Ehrenstein circle of Figs. 1A and 9, that are perpendicular or obliquely oriented with respect to line ends (Grossberg & Mingolla, 1985b, 1987). Cell activity for Competition 2 hypercomplex cells is governed by

$$\begin{aligned} \frac{d}{dt} y_{ijk} = & -Dy_{ijk} + (U - y_{ijk}) \sum_r C_{rk} T(w_{ijr}) \\ & - (y_{ijk} + L) \sum_r S_{rk} T(w_{ijr}) \end{aligned} \quad (26)$$

where interaction between cells at orientations k and r is defined by one-dimensional Gaussian kernels g_2 :

$$C_{rk} = Cg_1(r, k, \sigma_c) \quad (27)$$

$$S_{rk} = Sg_1(r, k, \sigma_s) \quad (28)$$

At equilibrium,

$$y_{ijk} = \frac{\sum_r (UC_{rk} - LS_{rk})T(w_{ijr})}{D + \sum_r (C_{rk} + S_{rk})T(w_{ijr})} \quad (29)$$

The output of Competition 2 is displayed in Fig. 18C. Because the output of Competition 1 has orientationally sharp responses for the example input, the sharpening of Competition 2 is not obvious. In addition, the endcuts in this example merely strengthen the direct filter responses at the (thick) line end. Parameter choices for eqn. (29) are $D = 1$, $U = 1$, and $L = 1$. Filter parameter for eqns. (27) and (28) are $C = 4.323$, $\sigma_c = 1.208$, $S = 4.323$, and $\sigma_s = 1.932$.

Bipole cells: Long-range cooperation

The cooperative stage sums input from two lobes of a bipole cell filter (Fig. 24E) that is activated by boundary signals from the previous hypercomplex cell stage. If there is sufficient activation in both lobes, feedback signals are generated that initiate boundary completion. The equation for this stage is

$$\frac{d}{dt} z_{ijk} = -z_{ijk} + f(A_{ijk}) + f(B_{ijk}) \quad (30)$$

where

$$f(x) = \frac{T(x)}{E + T(x)} \quad (31)$$

$$A_{ijk} = \sum_{p,q,r} (T(y_{ijr}) - T(y_{ijR}))T(Z_{pqij}^{(r,k)}) \quad (32)$$

and

$$B_{ijk} = \sum_{p,q,r} (T(y_{ijr}) - T(y_{ijR}))T(-Z_{pqij}^{(r,k)}) \quad (33)$$

In eqns. (31) and (32), R is the orientation perpendicular to r . The new bipole filter is defined by

$$\begin{aligned} Z_{pqij}^{(r,0)} = & Z \operatorname{sgn}(p - i) \\ & \times \exp\left(\frac{-(D_{pqij} - \rho)^2}{2\sigma_1^2} - \frac{F_{pqij}^2}{2\sigma_2^2} - \frac{\left(\frac{r\pi}{K} - F_{pqij}\right)^2}{2\sigma_3^2}\right) \end{aligned} \quad (34)$$

where

$$D_{pqij} = \sqrt{(p - i)^2 + (q - j)^2} \quad (35)$$

and

$$F_{pqij} = \tan^{-1}\left(\frac{p - i}{s - (q - j)}\right), \quad s \neq q - j \quad (36)$$

Variable s in eqn. (36) is given by

$$s = \frac{(p - i)^2 + (q - j)^2}{2(q - j)} \quad (37)$$

The first term in the exponential of eqn. (34) modulates filter values based on their distance D_{pqij} from the bipole's center, where ρ is the optimal distance from the center. The second term computes the slope of the tangent at (p, q) of the circle centered at $(0, s)$ which passes through $(0, 0)$ (the bipole cell's origin) and (p, q) ; see Fig. 23. This circle has equation

$$p^2 + (q - s)^2 = s^2 \quad (38)$$

and by implicit differentiation its tangent is

$$\frac{dq}{dp} = \frac{p}{s - q} \quad (39)$$

Note that the radius s will vary from point to point. The second term in the exponential penalizes orientations in the filter that have large tangent values. The most favorable orientations (for this term) are those similar to the bipole's main axis. The third term of eqn. (34) measures the similarity of the orientation of point (p, q, r) and the angle formed by the tangent at that point. The tangent defines the optimal orientation for that point. Filter element orientations closer to this optimal value will have greater strength than those at larger angular separations.

At equilibrium, the unthresholded bipole cell activity is, by eqns. (30)-(33),

$$\begin{aligned} z_{ijk} = & f\left(\sum_{p,q,r} [T(y_{pqr}) - T(y_{pqR})]T(Z_{pqij}^{(r,k)})\right) \\ & + f\left(\sum_{p,q,r} [T(y_{pqr}) - T(y_{pqR})]T(-Z_{pqij}^{(r,k)})\right) \end{aligned} \quad (40)$$

The new filter is consistent with the data of Field et al. (1993) and of Kellman and Shipley (1991). The new equation is also more easily modified and scaled than the original of Grossberg and Mingolla (1985b) because all of the terms are contained within a single exponential function. A similar bipole cell equation, based on parabolas instead of circles, was used by Cruthirds et al. (1992). The change to circles simplifies the equation as much as possible.

The output for this stage (Fig. 18D) shows where boundary enhancement and completion take place. The boundaries of the long (horizontal) side of the bars are long enough to stimulate horizontal bipole cells, as well as some oblique angle bipoles. In addition, the short, vertical boundaries of the bars are able to stimulate vertical bipole cells that lie in the gap between the lines. These vertical activations will ultimately give rise to two

boundaries connecting the lines at their ends. Parameter values for eqns. (31) and (34) are $E = 0.15$, $Z = 1$, $\sigma_1 = 4.0$, $\rho = 10.0$, $\sigma_2 = 0.3$, and $\sigma_3 = 0.1$.

In an image processing application of BCS/FCS mechanisms, Grossberg et al. (1994b) employed a variation in the bipole weighting function where $\rho = 0$, resulting in the strongest "weights" at locations near the bipole center. Such an arrangement allows bipole activity to remain strong from interiors of segments right up to endpoints, while still preventing outward completion beyond inducers.

Top-down orientation competition

This stage is homologous to Competition 2. It is called Competition 2F, with the 'F' indicating that the competition is in the feedback portion of the CC Loop. This stage, which was not included in the original BCS, sharpens boundary completions that have components from several orientations by enhancing the orientations at each point that are most highly favored by the cooperation. The equation for this stage is given by

$$\begin{aligned} \frac{d}{dt} u_{ijk} = & -Du_{ijk} + (U - u_{ijk}) \sum_r C_{rk} H(z_{ijr}) \\ & - (u_{ijk} + L) \sum_r S_{rk} H(z_{ijr}). \end{aligned} \quad (41)$$

where

$$C_{rk} = Cg_1(r, k, \sigma_c) \quad (42)$$

$$S_{rk} = Sg_1(r, k, \sigma_s) \quad (43)$$

$$H(z) = HT(z - J) \quad (44)$$

The signal function $H(z)$ determines whether a cooperative bipole cell is activated enough by both of its receptive fields to generate output signals that participate in the competition. At equilibrium,

$$u_{ijk} = \frac{\sum_r (UC_{rk} - LS_{rk})H(z_{ijr})}{D + \sum_r (C_{rk} + S_{rk})H(z_{ijr})} \quad (45)$$

The output of Competition 2F is shown in Fig. 18E. Normally this competition reduces the orientational spread of the cooperative signals, as in the complex imagery processed in Grossberg et al. (1994b). In the present example, however, most of the input signals are already orientationally as sharp as possible. The effects of sharpening can be seen by examining the pixels in the middle of each bar. Parameter values for eqns. (41) and (44) are $D = 1$, $U = 1$, $L = 1$, $H = 1$, and $J = 1.2$. Filter parameters in eqns. (42) and (43) are $C = 4.95$, $\sigma_c = 0.865$, $S = 4.95$, and $\sigma_s = 1.385$.

Top-down spatial competition

This feedback stage is homologous Competition 1, hence it is called Competition 1F, in that it occur across position within

each orientation. The feedback signals are spatially sharpened in this stage before being added back into the loop, as in

$$\begin{aligned} \frac{d}{dt} v_{ijk} = & -Dv_{ijk} + (U - v_{ijk}) \sum_{p,q} C_{pqij}^{(k)} T(u_{pqk}) \\ & - (v_{ijk} + L) \sum_{p,q,r} S_{pqij}^{(k)} T(u_{pqk}) \end{aligned}$$

where

$$C_{pqij}^{(0)} = Cg_3(p, q, i, j, \sigma_c, \sigma_g)$$

$$S_{pqij}^{(0)} = Sg_3(p, q, i, j, \sigma_s, \sigma_h)$$

and g_3 is defined by

$$g_3(p, q, i, j, \sigma_1, \sigma_2) = (2\pi\sigma_1\sigma_2)^{-1} \exp\left\{-\frac{1}{2}\left(\left(\frac{p-i}{\sigma_2}\right)^2 + \left(\frac{q-j}{\sigma_1}\right)^2\right)\right\} \quad (49)$$

When $\sigma_g \neq \sigma_c$ or $\sigma_h \neq \sigma_s$ the filters are anisotropic, taking an elliptical shape, as in Fig. 24F. When this is the case, rotated versions of the filters are applied within each orientation. This filter responds well to a line of activity while at the same time limiting the thickness of the line. At equilibrium,

$$v_{ijk} = \frac{\sum_{p,q,r} (UC_{pqij}^{(k)} - LS_{pqij}^{(k)})T(u_{pqr})}{D + \sum_{p,q,r} (C_{pqij}^{(k)} + S_{pqij}^{(k)})T(u_{pqr})}$$

The output of this stage (Fig. 18F) is a sharper version of its input wherein many of the flanking pixels in Fig. 18E have disappeared or been substantially weakened. Parameter values for eqn. (46) are $D = 1$, $U = 1$, and $L = 1$. Filter parameters for eqns. (47) and (48) are $C = 47.6$, $\sigma_c = 0.95$, $\sigma_g = 1.0$, $S = 120.0$, $\sigma_s = 1.0$, and $\sigma_h = 1.0$.

Boundary completion

The output of Competition 1F is fed back into Competition 1 [eqn. (21)] to close the CC Loop. Cooperative boundaries are added to the bottom-up boundaries in Competition 1, and the circuit computes the completed boundaries, including illusory contour boundaries, of the input image. The output of the CC Loop is the equilibrium activation of Competition 2 (Fig. 18G). These completed boundaries are sharply localized at the correct spatial positions. They are used in the FCS to contain the spreading of brightness signals.

Filling-in

The brightness signals that fill-in this stage are derived from the ON and OFF channels of the LGN stage. As noted in Cohen and Grossberg (1984) and Grossberg & Todorović (1988), filling-in uses the ON and OFF signals to recover a surface reconstruction that is relatively uncontaminated by variations in illumination. Filling-in occurs separately *via* nearest-neighbor

diffusion in ON and OFF filling-in domains, or FIDOs. The final output is the difference of the ON and OFF FIDO activations at each location, hence a double-opponent response (Grossberg, 1987*b*; Grossberg & Wyse, 1991). The FIDOs are two-dimensional isotropic networks, so that filling-in proceeds equally in all directions until it is blocked by a boundary or attenuated with distance.

Cell activity in each syncytium is described by a diffusion equation

$$\frac{d}{dt} s_{ij} = -Ds_{ij} + T(r_{ij}) + \sum_{p,q \in N_{ij}} (s_{pq} - s_{ij})P_{pqij} \quad (51)$$

in which a FIDO cell s_{ij} receives input from LGN cell activity r_{ij} , as defined by eqn. (12), and from FIDO cells in the neighborhood

$$N_{ij}\{(i, j - 1), (i - 1, j), (i + 1, j), (i, j + 1)\} \quad (52)$$

The conductance coefficient P_{pqij} between two neighboring cells depends on the strength of the boundary between them:

$$P_{pqij} = \frac{\delta}{1 + \epsilon(Y_{pq} + Y_{ij})} \quad (53)$$

where the equilibrium BCS boundaries from Competition 2 of eqn. (29) are summed over orientation:

$$Y_{ij} = \sum_k T(y_{ijk}) \quad (54)$$

The equilibrium ON and OFF syncytial activities are the solutions to the sets of simultaneous equations defined, respectively, by

$$s_{ij}^+ = \frac{T(r_{ij}^+) + \sum_{p,q \in N_{ij}} s_{pq}^+ P_{pqij}}{D + \sum_{p,q \in N_{ij}} P_{pqij}} \quad (55)$$

and

$$s_{ij}^- = \frac{T(r_{ij}^-) + \sum_{p,q \in N_{ij}} s_{pq}^- P_{pqij}}{D + \sum_{p,q \in N_{ij}} P_{pqij}} \quad (56)$$

The final filled-in double-opponent output f_{ij} , shown in Fig. 19, is calculated by subtracting the OFF channel output from the ON channel output:

$$f_{ij} = s_{ij}^+ - s_{ij}^- \quad (57)$$

Default parameter values for the filling-in eqns. (51) and (53) are $D = 0.001$, $\delta = 1000$, and $\gamma = 10000$.

Computer implementation

The computer implementation of the BCS/FCS model is written in C and runs on a Silicon Graphics Iris 4D/28OS machine. The equilibrium equations for each stage are used. The LGN feedback loop is computed by cycling once through the relevant stages, giving the following order of processing: Retinal stage, LGN stage with no feedback, Complex Cells, Competition 1, LGN stage with feedback, Complex Cells, CC Loop, Filling-in.

The CC Loop is computed by cycling multiple times through the equilibrium equations for Competition 1, Competition 2, Cooperation, Competition 2F, and Competition 1F, in that order. The cycle ends when there is no significant change in the values of Competition 1 from the previous cycle. Five cycles are often sufficient, translating to a runtime of about 5 min for a 128×128 image.

The accuracy of the CC Loop approximation was checked by integrating the dynamic equation for Competition 1 (while solving the other stages at steady state) using the LSODA software integration package (Petzold, 1983). At convergence, the results were indistinguishable from those obtained by the iterative method described above. A similar test of the LGN stage yielded equally good results. In both cases, integration takes much longer than the respective approximations.

In order to achieve a better discrete approximation of filter functions than could be obtained by evaluation at a single pixel, several subpixel calculations were used. For example, the kernels of eqn. 3 centered at location (p, q) were evaluated in the range $p - 0.5$ to $p + 0.5$ in increments of 0.1, and similarly for q values. The average of all these evaluations was used to compute ON and OFF cell responses.

Index variables r and k , used to denote orientational tuning, are implicitly modular. Their values "wrap around" at the number of discrete orientations used in the simulations. Thus, to compute cross-orientation competition for 12 orientations, values of $r-k$ must always be between -5 and 5 . If $r-k$ is not in this range, 12 is added or subtracted, as necessary.

For the sake of visual clarity, the display of the simulated output of eqns. 21-25, shown in Fig. 18B, does not show activity in locations whose only positive input is that of the tonic excitation, J .